Activation Rate of Seismicity for Hydraulic Fracture Wells in the Western Canada Sedimentary Basin

Hadi Ghofrani*[1] and Gail M. Atkinson[1]

ABSTRACT

The rate of M ≥ 3 earthquakes associated with hydraulic fracturing (HF) in horizontal wells (HF wells) in the Western Canada Sedimentary Basin is estimated for the period from 2009 to 2019. The estimates are based on a statistical discrimination algorithm that uses an objective scoring function deduced from the observed spatiotemporal correlations between wells and earthquakes. A Monte Carlo simulation approach is used to test the efficacy of the scoring function in determining noncoincidental association rates, allowing for correction of the observed association rates for the expected number of false positives. The basin-wide average rate of association of M ≥ 3 earthquakes with HF wells (2009–2019) is ~0.8% on a per well basis. The susceptibility appears to vary by formation by more than an order of magnitude, ranging from ~6% for HF wells in the Duvernay Formation to ~0.07% for HF wells in the Cardium Formation. For some formations, there has been no observed association at the M ≥ 3 level to date, but this does not necessarily imply that such formations are immune to induced seismicity.

KEY POINTS

- The rate of **M** ≥ 3 earthquakes per HF well in the WCSB is determined regionally and by formation.
- The average **M** ≥ 3 rate per HF well is ~0.8% regionally, varying by formation by more than a factor of 10.
- Estimated rates can be used to forecast induced seismicity hazard associated with hydraulic fracturing.

INTRODUCTION

This study characterizes the empirical correlation between seismicity and hydraulic fracturing (HF) in horizontally drilled wells (HF wells) in the Western Canada Sedimentary Basin (WCSB). Seismicity in the WCSB increased markedly (factor of ~4) starting in about 2009, synchronous with a large increase (factor of ~10) in the number of hydraulic fracture treatments completed in horizontal wells (Atkinson *et al.*, 2016). In a previous study (Atkinson *et al.*, 2016), we analyzed the statistics of seismicity in the WCSB in relation to oil and gas activities between 1985 and 2014, considering both HF wells and fluid disposal wells. The key finding was that the rate of earthquakes increased synchronously with the increase in HF wells, starting in 2009. By analyzing the spatiotemporal correlation of earthquakes and oil and gas activities, we concluded in 2016 that, on average, ~0.3% of HF wells and ~1% of disposal wells are associated with moment magnitude **M** ≥ 3 earthquakes. We also showed that most of the recent seismicity in the WCSB (about 60% of all events) is associated with HF wells. These two conclusions are mutually consistent because HF wells greatly outnumber disposal wells (by about a factor of 50 to 1; Fig. 1).

The findings of Atkinson *et al.* (2016) in the WCSB were considered novel because increased rates of seismicity in the central United States, to that point, had been attributed almost entirely to wastewater disposal (e.g., Ellsworth, 2013; Rubinstein and Babaie Mahani, 2015; Weingarten *et al.*, 2015). The apparent differences between observations in the WCSB, where HF-induced events predominate, and those in the central United States, where disposal-induced events predominate, are now better understood. In the WCSB, the sharp increase in HF wells has not required a correspondingly sharp increase in the number of disposal wells, in part because the WCSB does not include large dewatering plays that require the subsequent disposal of massive volumes of coproduced wastewater (Rubinstein and Babaie Mahani, 2015). Large-scale transfers of formation fluids are a key characteristic of oil

1. Department of Earth Sciences, Western University, London, Ontario, Canada
*Corresponding author: hghofra@uwo.ca

Cite this article as Ghofrani, H., and G. M. Atkinson (2020). Activation Rate of Seismicity for Hydraulic Fracture Wells in the Western Canada Sedimentary Basin, *Bull. Seismol. Soc. Am.* **110**, 2252–2271, doi: 10.1785/0120200002

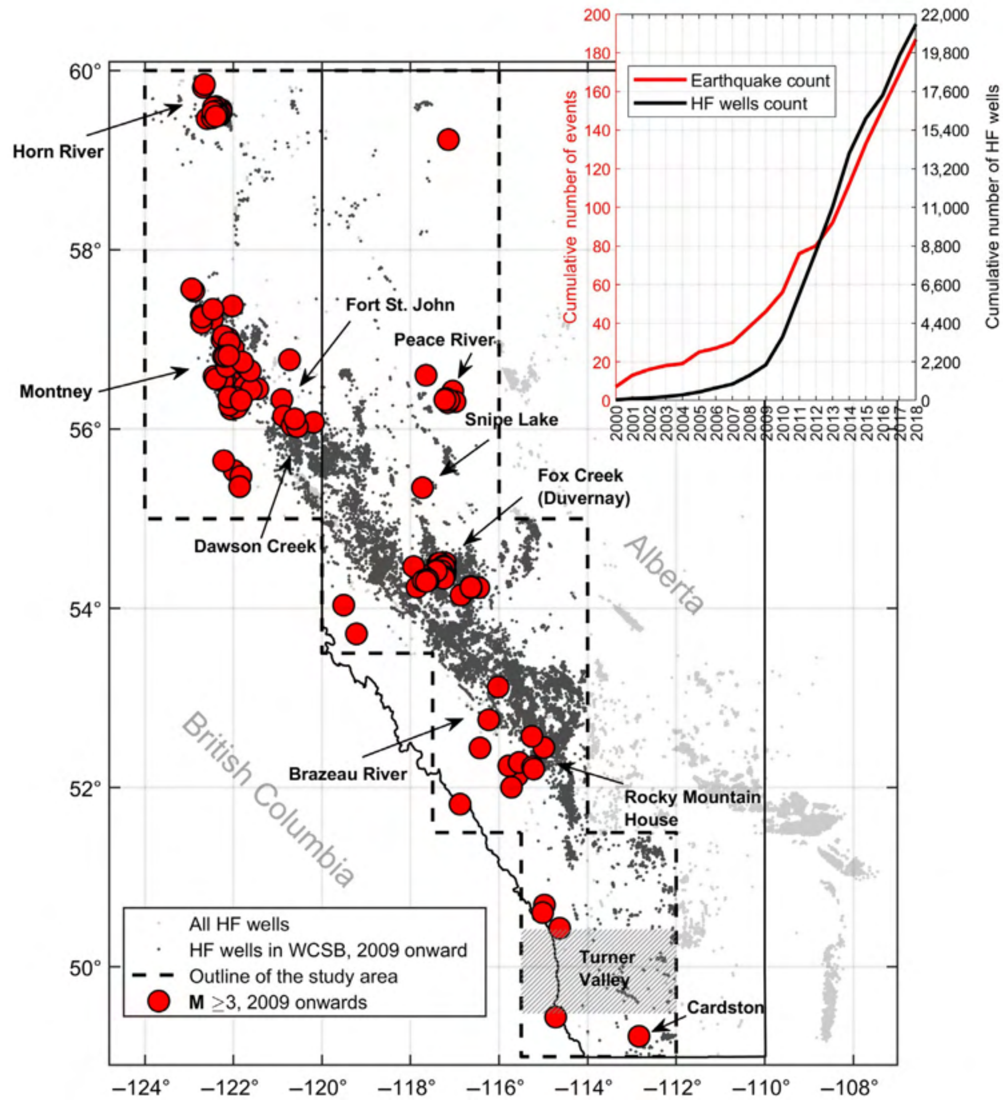

Figure 1. Seismicity of moment magnitude (**M**) ≥ 3 from 2009 to April 2019 (large circles) and hydraulic fracturing (HF) wells (small circles, with darker symbol showing those active from 2009 to April 2019). Dashed black lines delineate the study area, which parallels the foothills region of the Western Canada Sedimentary Basin (WCSB). The shaded area, which is near the Turner Valley, is excluded from the study due to contamination of the earthquake catalog with undistinguished blasts (see the Observed Relationship between HF Wells and Earthquakes section). The inset shows the cumulative number of **M** ≥ 3 earthquakes and HF wells in the WCSB from January 2000 to April 2019. The color version of this figure is available only in the electronic edition.

production in parts of the central United States, particularly Oklahoma (Murray, 2013; Walsh and Zoback, 2015; Weingarten *et al.*, 2015) but not in the WCSB. Consequently, there has been a much greater increase in wastewater disposal in the central United States relative to that in the WCSB, along with an even greater increase in seismicity rates—by a factor of ~10 in the United States (Ellsworth, 2013) versus ~4 in the WCSB. The prevalence of disposal-induced seismicity in the central United States has the effect of masking HF seismicity. But in recent years, several studies have shown that HF seismicity also occurs frequently in oil and gas regions of the central United States, including Ohio (Friberg *et al.*, 2014; Skoumal *et al.*, 2015), Oklahoma (Holland, 2013; Skoumal *et al.*, 2018), and Texas (Lomax and Savvaidis, 2019).

The association rates of HF wells with significant seismicity vary widely within and across regions. Atkinson *et al.* (2016) reported a basin-wide average incidence of ~0.3% per well for the WCSB. Ghofrani and Atkinson (2016) reported a similar average rate for the WCSB but also noted that the rate was higher than the regional average by a factor of ~4 for regions within ~20 km of Devonian reef complexes identified by Schultz *et al.* (2016) as markers for likely basement faulting (and lower than average in other regions). Skoumal *et al.* (2018) identified 16 regions within Oklahoma where HF wells were associated with seismicity. In some of these regions, >50% of HF wells correlated with seismicity, explaining over 95% of the observed seismicity. By contrast, many regions (e.g., the Bakken play in the Williston basin) have experienced widespread increases in both HF and disposal wells with negligible associated seismicity (Ellsworth *et al.*, 2015). In summary, based on previous examples in the literature, association rates of seismicity with HF wells may vary from rates too low to reliably measure to rates as high as 50% in some localized areas.

In this study, we revisit the association between seismicity and HF wells in the WCSB using improved information on both HF well treatments and earthquakes from January 2009 to April 2019. Figure 1 shows the locations of HF wells (bottom-hole coordinates) and **M** ≥ 3 earthquakes in our study database; this is the same geographic region considered by Atkinson *et al.* (2016), which parallels the foothills region of the WCSB. The new database enables the development of an objective scoring function to estimate the likelihood of association based on the spatiotemporal relationships between HF well treatments and $\mathbf{M} \geq 3$ earthquakes. A Monte Carlo simulation approach is used to test the efficacy of the scoring function and to allow for correction of the observed association rates for the expected number of false positives (i.e., coincidental associations). The improved database also allows us to subdivide the association rates by geological formation within the WCSB. It is widely agreed that some formations within the WCSB, such as the Duvernay and Montney, are particularly susceptible to induced seismicity (e.g., Corlett *et al.*, 2018; Eaton and Schultz, 2018), but the susceptibility of other formations is not yet well documented. Documenting these correlations is a first step toward understanding the reasons for the differences and their implications for induced seismicity processes.

This article advances the work presented in Atkinson *et al.* (2016) in several significant respects:

1. we incorporate 4 yr of new information on HF wells and seismicity, including significant new earthquakes such as those near Fort St. John (2018 **M** 4.6), Fox Creek (2016 **M** 4.1 and several new $\mathbf{M} \geq 3$), and Red Deer (2019 $\mathbf{M} \sim 4$);
2. our HF well database is much more complete than that available in 2015, containing more accurate information on the start and stop dates of HF treatments; this enables development of more robust correlations between seismicity and HF wells;
3. we use histograms of time lags and distance offsets between HF wells and earthquakes to develop an objective scoring function expressing the likelihood of association of HF wells with $\mathbf{M} \geq 3$ seismicity;
4. we use a statistical approach to handle cases for which more than one well might reasonably be associated with observed seismicity, rather than trying to tag a specific HF well as the culprit in ambiguous cases; and
5. we examine the per-well association rate between HF wells and $\mathbf{M} \geq 3$ earthquakes subdivided by geologic formation.

As in Atkinson *et al.* (2016), our goal is to provide a regional-scale overview of the association rates between $\mathbf{M} \geq 3$ earthquakes and HF wells. These rate estimates are required for probabilistic analyses to examine the impact of induced seismicity on site-specific and regional seismic hazards (e.g., Atkinson *et al.*, 2015; Atkinson, 2017). We do not attempt to associate specific earthquakes with specific wells, nor do we address the causative mechanisms of HF-induced seismicity.

OBSERVED RELATIONSHIP BETWEEN HF WELLS AND EARTHQUAKES

The study database is shown in Figure 1. We use the earthquake catalog in the WCSB for the time period from 1 January 2009 to 30 April 2019 (obtained from Canadian Induced Seismicity Collaboration website; see Data and Resources), which contains event dates and locations, with all magnitudes converted to **M**. The Turner Valley area (see Fig. 1) is excluded from study because the catalog in this area is believed to be contaminated by undistinguished blasts due to sparse network coverage. The threshold magnitude of $\mathbf{M} \geq 3$ is chosen for the analysis because the catalog is considered complete above this level (Cui and Atkinson, 2016)—although there is always the possibility that a few events may be missed, especially near the beginning of the time period. Moreover, $\mathbf{M} \geq 3$ represents a significant level of ground shaking, likely to be felt at close distances (Atkinson *et al.*, 2015; Ghofrani *et al.*, 2019). There were 20,687 laterally stimulated HF wells within the WSCB study area during the study period; their locations, dates, and treatment formations were extracted using the geoSCOUT database and software (see Data and Resources).

To examine the spatial correlation between HF wells and seismic events, Atkinson *et al.* (2016) performed an initial screening to flag all $\mathbf{M} \geq 3$ earthquakes having a reported location within a 20 km radius of an HF well. That deliberately broad distance was chosen based on the following considerations: (1) the typical location uncertainty of catalog events is ~10 km in many areas of the WCSB, as evidenced by discrepancies in event locations quoted by different agencies for the same events; (2) multistage HF wells may be several kilometers in lateral extent; and (3) events may be induced at distances up to a few kilometers from the causative well (Schultz, Mei, *et al.*, 2015; Schultz, Stern, *et al.*, 2015; Bao and Eaton, 2016). A broad timing criterion was also adopted by Atkinson *et al.* (2016), based on literature studies, flagging all earthquakes that occurred <92 days (3 months) following the initiation of the HF well treatment.

In this study, we start with the same flagging criteria as Atkinson *et al.* (2016), but we refine our criteria based on interpretation of the observed spatiotemporal relationships between events and wells, as illustrated in Figure 2. The initial screening flags 111 of 152 events of $\mathbf{M} \geq 3$. These events could potentially be associated with up to 693 HF wells, out of a total of 20,687 HF wells in the database. In evaluating the proximity of events to wells, we need to consider the earthquake location uncertainty in the region, which is approximately 10 km for the study period (Schultz *et al.*, 2017; Eaton and Schultz, 2018); thus events that are calculated to be at a distance of 5–10 km from a well could potentially be occurring at significantly closer (or farther) distances. There is also ambiguity in the time with respect to the HF treatment. We calculate the time with reference to the initiation of HF operations at a well. Thus the shortest time lag refers to the occurrence of the first $\mathbf{M} \geq 3$ earthquake following initiation of HF operations. However, there could be multiple smaller events below our threshold that occurred before this first $\mathbf{M} \geq 3$. Moreover, by examining a histogram of the elapsed time between the initiation and completion of HF treatments for the wells in our database, we observed that ~85% of HF wells have stimulation periods in the range from 1 to 10 days. However, there is a long

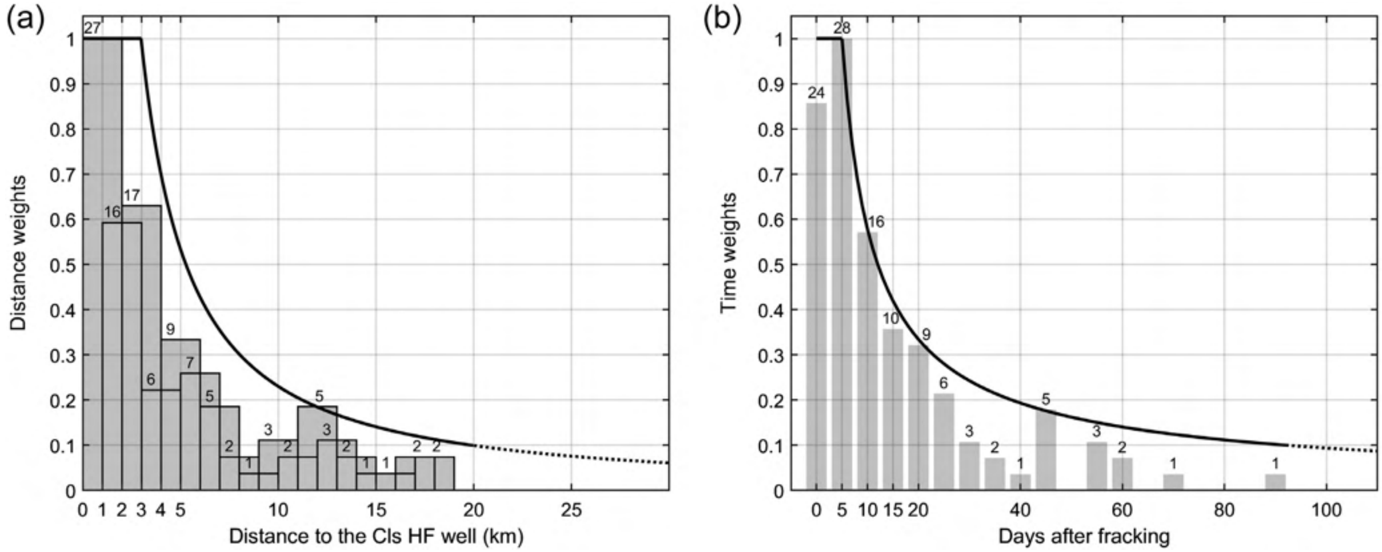

Figure 2. Distribution of (a) distance to the closest (Cls) HF well (i.e., shortest distance offsets) and (b) shortest time lags of HF wells associated with **M** ≥ 3 events flagged in the initial screening. The numbers over each bar represent the number of elements in each distance or time bins. The solid curves show the adopted weight functions to represent the distributions (see the Observed Relationship between HF Wells and Earthquakes section). The extensions of the model beyond the initial screening criteria are shown as dotted lines. Larger bar widths for the distance distribution are used to reflect uncertainty in locations.

tail, with some HF durations extending to 90 days. This reflects industry practice in which stimulation is performed in multiple stages—usually over a period of several days but sometimes with significant downtime between stages. We believe that the time lags shown in Figure 2, when considered in parallel with the duration of stimulation periods, are consistent with observations made in other regions. Specifically, most events occur during the treatment window (e.g., Skoumal *et al.*, 2015, 2018) or shortly thereafter. However, in some instances larger events may occur days to weeks after stimulation has ended (e.g., Bao and Eaton, 2016). To our knowledge, there is no accepted cutoff interval beyond which an event cannot have been triggered; rather, there is a decreasing probability of association after the stimulation period ends.

Figure 2 shows that most events flagged in the initial screening have an HF well within ~8 km and have been stimulated within the 20 day window preceding the event. Specifically, ~70% of **M** ≥ 3 epicenters are within 5 km of an active HF well and ~84% of epicenters are within 10 km. Approximately 41% of flagged **M** ≥ 3 events are associated with HF treatments that commenced within the preceding 5 days, ~60% within 10 days, and ~77% within 20 days. It should be emphasized that, based on the typical duration of HF operations, this means that most of the activity occurred during the stimulation period. It is an interesting observation that both the time and distance scales in which most of the events are shown to occur (Fig. 2) are generally consistent with the overall areal extent of HF wells (i.e., several kilometers in lateral extent) and the typical duration of operations (days to weeks). Moreover, both the spatial and temporal distributions show a rapid initial decline as distance and time increase, which is the behavior expected if the events are associated with the wells. By contrast, beyond about 8 km and 30 days, the distributions appear relatively uniform, which is the behavior expected if the events are random with respect to the wells. Our observation that most events flagged as potentially associated have an HF well within ~8 km, at which HF operations commenced within the preceding 20 days, is generally consistent with the results of others, despite differences in the discrimination methodologies used. For example, Skoumal *et al.* (2018) use a discrimination algorithm to identify HF wells in Oklahoma that exhibit changes in seismicity rates over a range of time and distance scales with respect to the HF treatments. Following this initial flagging, they further examine cases in which events occurred within 7 km and 7 days of the stimulation timeframe. A key difference in our study and that of Skoumal *et al.* (2018), which motivates our approach, is in the geographic scale considered and the completeness of the regional seismicity catalog. Because we are considering only events of **M** ≥ 3, the seismicity is very sparse in time and space, making individual correlations with nearby wells inherently uncertain.

We model the histograms as distributions having a steep decline followed by a tail (beyond 8 km and 30 days) that contains up to 20% of the distribution. These distributions can be interpreted as weight functions that reflect the relative likelihood of association based on the observed statistical behavior. We define the weight functions from an empirical fit to the following (shown in Fig. 2):

$$w_d(D) = \begin{cases} 1.0 & D \le 3 \text{ km} \\ 3.794D^{-1.2137} & D > 3 \text{ km} \end{cases}, \quad (1)$$

$$w_t(T) = \begin{cases} 1.0 & T \le 5 \text{ days} \\ 3.5696T^{-0.79063} & T > 5 \text{ days} \end{cases}, \quad (2)$$

in which D and T are the distance offset (in kilometers) and time lag (days), respectively, of an HF well with respect to an $\mathbf{M} \ge 3$ event. We set the functional form of the weight equations based on the shape of the distance and time distributions. The idea is to model the overall trend of the empirical observations in a simple way while avoiding overfitting. We use a trust region algorithm for nonlinear least-squares problems to find the power law exponents in equations (1) and (2).

We combine the two weight functions (equations 1 and 2), taking the average value as the final score (e.g., following Walter *et al.*, 1995):

$$W = [w_d(D) + w_t(T)]/2. \quad (3)$$

The discriminant score W, which varies in the range from 0 to 1, can be interpreted as a measure of the likelihood that an HF well is associated with an $\mathbf{M} \ge 3$ event. We did not assign an absolute cutoff distance or time for the distributions. We recognize that the flagged events within the tails of the distribution (values of <0.2 in Fig. 2) are most likely to be false positives (i.e., coincidental associations) but might also indicate some triggering potential beyond ~8 km (accounting for mislocation) and/or beyond ~20 days (accounting for extended stimulation intervals). Wells with $W < 0.15$ are not considered further for potential association.

The distance and time scoring functions could be interpreted in light of multiple mechanisms that may be involved in the process of inducing an event, including the reduction of effective stress on faults due to elevated pore pressure, fault loading by poroelastic stress transfer, and stress transfer by aseismic slip (Eaton, 2018). The functions suggest that the probability of association is decreasing as a power law in both time and distance. This observation is in agreement with Omori's law (see Utsu *et al.*, 1995), which has been related to diffusion of pore pressure (Nur and Booker, 1972; Langenbruch and Shapiro, 2010). Events triggered by pore-pressure diffusion should result in high weights at short distances with a sharp decay trend, because most studies suggest that pore pressure diffusion is unlikely to be a significant triggering mechanism for HF at distances much beyond the footprint of the treatment zone due to the low formation permeabilities. At greater distances, stress transfer—by either Coulomb stress (e.g., Catalli *et al.*, 2013; Pennington and Chen, 2017; Brown and Ge, 2018) or aseismic slip (e.g., Guglielmi *et al.*, 2015; Viesca, 2015; Eyre *et al.*, 2019)—is a more likely mechanism, particularly if the time lag is short and the distance is large (several kilometers). We are hesitant to overinterpret the histograms of Figure 2 in terms of causative mechanisms because we believe that such interpretations are better left to analyses conducted on a finer scale with more detailed data. In particular, the power-law falloff with distance may be significantly affected by location uncertainties, whereas the power-law falloff with time is affected by the duration of the stimulation period.

In the initial screening, a uniform likelihood was implicitly assumed for distance and time values over the given ranges (20 km and 92 days). In the context of the current study, this could be considered an a priori distribution. The weight functions provide posterior distributions for the distance offsets and time lags of the HF wells associated with $\mathbf{M} \ge 3$ events within a Bayesian framework. We caution that the weighting functions provide a crude likelihood distribution that is intended to be used in an aggregate sense, not as a discriminant tool to determine the likelihood that specific individual earthquakes were induced by specific wells.

For many earthquakes, there is more than one well that passed the initial screening for potential association. The distributions plotted in Figure 2 were based on the closest HF well and the shortest elapsed time after initiation of HF operations for such cases. This greatly reduced the number of wells considered in constructing the distribution (111) relative to the number that were initially flagged (693). Moreover, it should be noted that the HF well at the closest distance may not be the same as the HF well with the shortest time lag, and thus the associations are not unique. In constructing Figure 2, our sole purpose was to elucidate the spatiotemporal distributions of seismicity with respect to HF wells. It was not our intent to associate each earthquake with a specific HF well.

The nonuniqueness of association between HF wells and events is an interesting and significant issue. Figure 3 illustrates a typical case in which we might flag one HF well as being the most likely culprit for association based on its close relationship in space (equation 1), whereas we might flag another based on its close relationship in time (equation 2). Moreover, if we consider the combination of space and time (equation 3), we might flag a different culprit. In many cases, there may be more than one well having a very similar W score, such as wells 2 and 3 in Figure 3. Finally, there may be cases for which two wells were involved in triggering an event. As a hypothetical example, suppose two wells were stimulated at the same time and at the same distance with respect to an associated event. It might be the combined effects of stress perturbations from the two wells that triggered the event.

In Figure 4, we plot the score function W as a function of distance and time. The largest score is obtained for HF wells within 3 km and 5 days of an epicenter. The value of the score W declines sharply as distance and time with respect to an $\mathbf{M} \ge 3$ event increase. We could adopt several alternative approaches for identifying possible culprit wells. The most obvious approach might be to consider the well with the highest score above some threshold as the culprit well, with its strength of association being given by its value. For example, an HF well within 3 km and 5 days would get a weight of 1 and

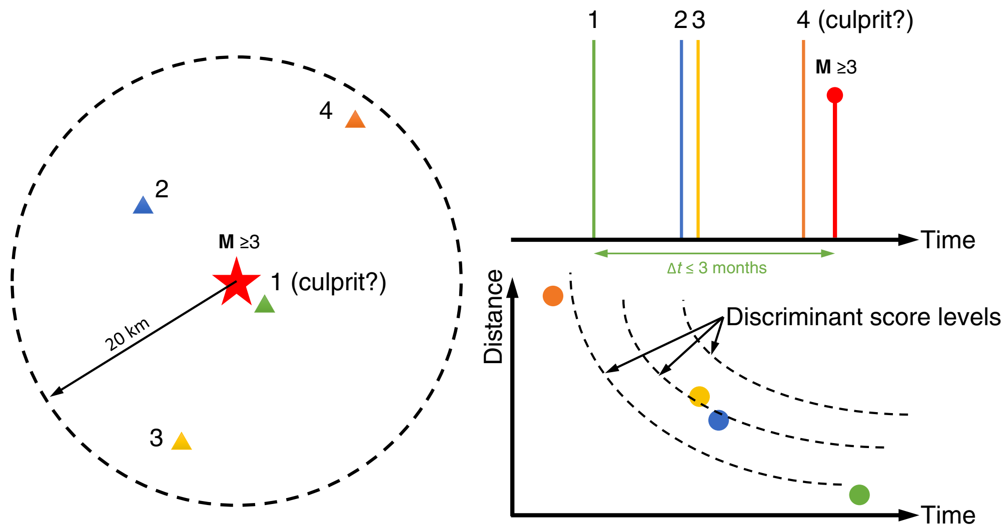

Figure 3. Conceptual diagram of potential association of **M** ≥ 3 earthquake with multiple HF wells, showing spatial and temporal distributions (i.e., distance offsets and time lags). Triangles are example HF wells and the vertical bars are their corresponding start time with respect to an **M** ≥ 3 event. For identifying a potential culprit well, there are several options: well 1 (considering distance as the discriminant parameter; equation 1); well 4 (considering time as the discriminant parameter; equation 2); well 2 (considering maximum score *W*, in which the effects of time and distance are averaged to define a discriminant parameter; equation 3). The color version of this figure is available only in the electronic edition.

would likely represent a unique association. However, as noted previously, there may be multiple wells that meet the initial screening criteria and have similar W scores. This suggests that the potential role of an HF well in triggering the seismicity should be viewed as an assessment of relative likelihood.

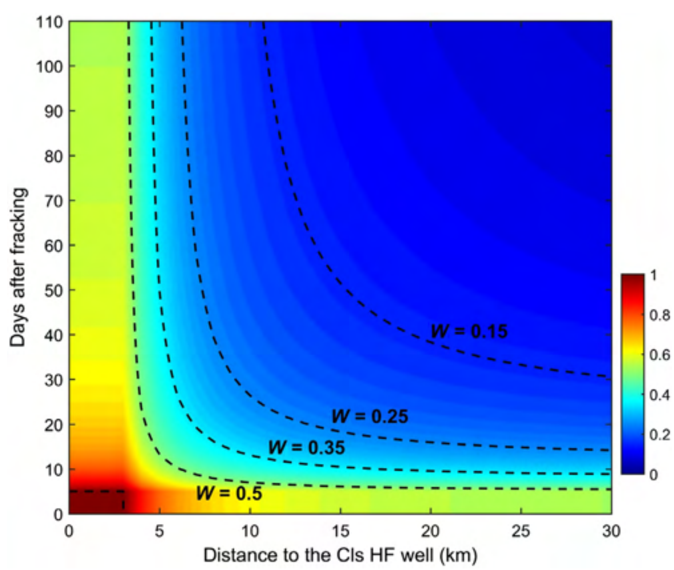

Figure 4. 2D plot showing the total discriminant score *W* for **M** ≥ 3. Dashed lines represent specific score values; shading shows a continuous spectrum of scores as a function of distance and time, with darker shading representing higher scores. The color version of this figure is available only in the electronic edition.

For example, if there are two nearby wells that might be associated with an **M** ≥ 3 event, each at 5 km and 12 days (Figs. 2 and 3), they would each get a weight of 0.5. Based on the distributions shown in Figures 3 and 4, we consider wells having a score of $W \geq 0.35$ as passing a reasonable threshold for association; these are wells that, on average, are within 20 days and 8 km of an **M** ≥ 3 event. The choice of $W \geq 0.35$ as an optimal discriminant was motivated by a Monte Carlo analysis of the significance of various score values, as described in the next section. We acknowledge that there is an element of subjective judgement in this choice.

The discriminator function for the line defining $W = 0.35$ (i.e., $[w_d(D) + w_t(T)] = 0.7$) can be described by the following equation:

$$T = \left(\frac{0.7 - 3.794D^{-1.2137}}{3.5696}\right)^{-1.2648}. \quad (4)$$

This condition is met for a range of situations in which $5 \leq D \leq 20$ km and $10 \leq T \leq 92$ days (see Fig. 4). Based on this function, any well flagged in the initial screening (i.e., $D \leq 20$ km) that lies below the curve (i.e., was stimulated within time $\leq T$) is considered a hit for potential association; its relative likelihood of association will range from 0.35 to 1.0, depending on its location and treatment start date with respect to an **M** ≥ 3 event.

Figure 5 shows a few examples of the scoring function in action for specific earthquakes. For some events, there is more than one HF well at <4 km distance at which stimulation occurred within the preceding 5 days. These wells receive very high scores (near 1). For other events, there are several HF wells at ~5 km, with treatment start dates within the 10–20 day window. These potential associations receive scores of ~0.5.

We calculate the distances and time between all **M** ≥ 3 earthquakes and all HF wells in our database that passed initial screening and determine the discriminant scores W. The results are illustrated for all wells in Figure 6. Score contours representing values of 1.0, 0.5, 0.35, 0.25, and 0.15 are shown as reference; values of $W < 0.15$ are considered to have insignificant association. The advantage of using the scoring function is that we can assess the relative likelihood of association based

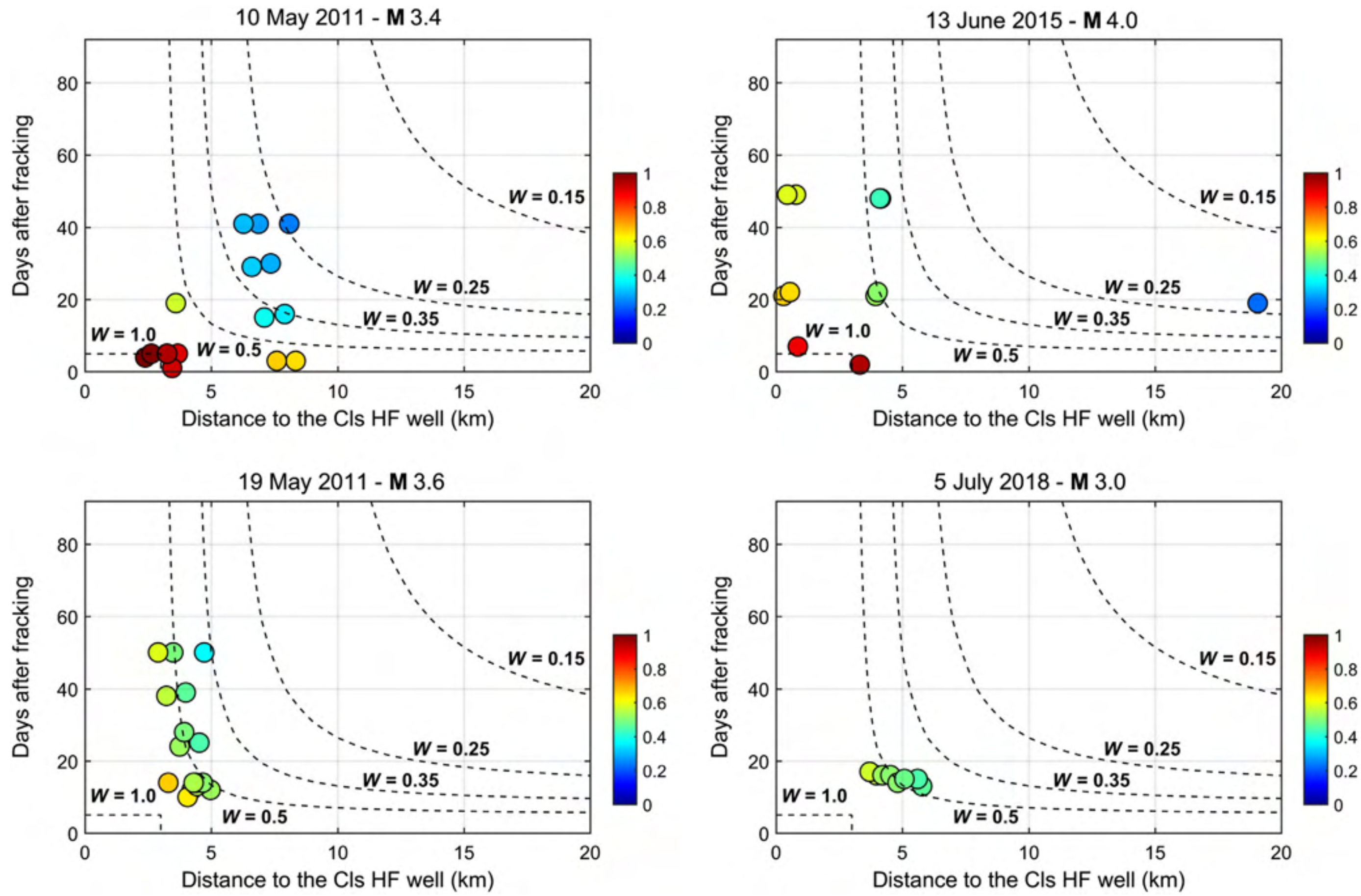

Figure 5. Performance of the scoring function *W* for some example events having multiple HF wells nearby. Shading represents the total score for each well with respect to the subject event (given in title line). Dashed lines represent specified *W* score values. The color version of this figure is available only in the electronic edition.

on the location and treatment start time of each HF well with respect to each **M** ≥ 3.0 event. Using the scoring function, HF wells passing initial screening are given relative likelihoods of association with an event based on their distance and start date. Table A1 lists all **M** ≥ 3 events for which there is at least one well with a discriminant score of ≥0.15.

We examined the performance of the weighting function for several high-quality datasets described in previous studies, as referenced in Table A1. For events within notable HF sequences that have been studied in detail such as those in central Alberta (Schultz, Mei, *et al.*, 2015; Schultz, Stern, *et al.*, 2015; Bao and Eaton, 2016; Schultz *et al.*, 2017; Eaton *et al.*, 2018), and northeastern British Columbia (B.C. Oil and Gas Commission, unpublished manuscript, 2012, 2014, see Data and Resources; Babaie Mahani *et al.*, 2019), we generally obtain a significant *W* score (>0.3). However, the discriminant scores vary depending on the availability and accuracy of well and seismicity information. For example, for the three events that occurred on 30 November 2018 in the Septimus region of northeast British Columbia, we estimated relatively modest *W* scores, in the range from 0.18 to 0.49, based on the well information in the public database. However, the study conducted by Babaie Mahani *et al.* (2019) had access to private industry data that confirmed that HF operations were in progress only 0.5 km away at the time of the first event. If this well information had been in the available database, the *W* score for the events would have been 1.

We also noted that there are known HF-induced sequences that are missed in Table A1. In particular, our algorithm did not flag the **M** 3.0 that was part of the Cardston swarm, a series of events in 2011–2012 in Alberta that were associated with HF completions. Closer investigation revealed that this event had not been detected by the regional network and thus was missing in our catalog; this likely occurred due to the sparse station coverage at that time. Based on the earthquake location in Schultz, Mei, *et al.* (2015), Schultz, Stern, *et al.* (2015), and publicly available well information, we would obtain $W = 0.73$ for that event. Our algorithm also did not flag the 9 March 2018 M_L 3.13 event and the 4 March 2019 M_L 4.18 event HF, both near Red Deer, Alberta (Schultz *et al.*, 2019), because they fell just outside our study area. Based on the currently available information, our algorithm would return a discriminant score of 0.7 for the 9 March 2018 event.

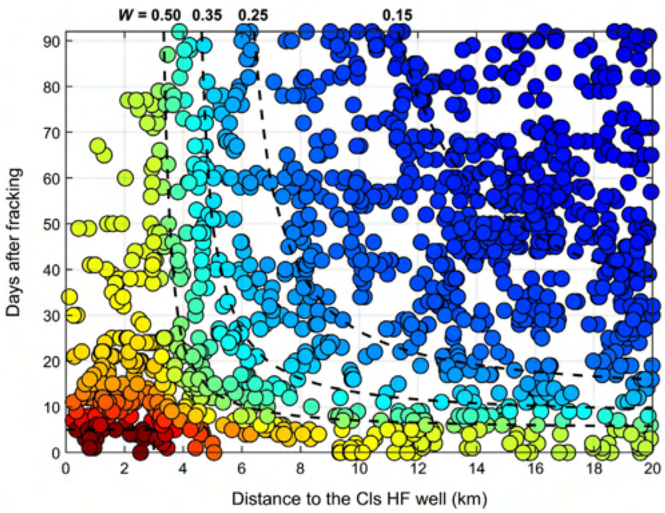

Figure 6. Values of the scoring function W for HF wells passing the initial screening criteria. Dashed lines represent scoring values of $W = 1.0$, 0.5, 0.35, 0.25, and 0.15. The color version of this figure is available only in the electronic edition.

For the 4 March 2019 event, our algorithm would return a W score of ~0.8 based on the estimated distance offset and time lag of the culprit HF well with respect to the event, as given by Schultz and Wang (2020). The March 2019 event is an example of an event for which the corresponding well information is still missing in the available database. This highlights that events can be missed by the algorithm due to incomplete or inaccurate information on earthquakes, wells, or both. Nevertheless, most notable sequences are identified with a significant W score, and there are many events identified that have not yet been studied in the literature.

SIGNIFICANCE OF THE OBSERVED ASSOCIATION OF M ≥ 3 WITH HF WELLS

It is clear from Figure 6 that using a higher W score as a discriminant for association will result in a smaller number of HF hits; however, it should also result in a smaller number of false positives (i.e., coincidental associations). This raises the question as to the optimal value of W to consider as being diagnostic of an association. We address this question by performing Monte Carlo simulations to determine the false positive rates expected for various values of W.

If the earthquakes are unrelated to the HF wells, then their timing with respect to well operations should be random. Accordingly, we simulate 5000 earthquake catalogs, each of which has 152 events distributed randomly in time over the same period. For the spatial distribution of events within each simulated catalog, we displace each earthquake by a random distance from 0 to 20 km, at a random azimuth, relative to its location in the real catalog. This maintains the overall clustering of seismicity in space but blurs individual event locations, in a manner analogous to the smoothed seismicity approach often used in seismic-hazard analysis (e.g., Frankel, 1995); in our case the distance scale of the smoothing is motivated by our initial flagging criteria. By perturbing the locations of the earthquakes in our simulated catalogs, we seek to minimize potential bias of the results that could result from holding the earthquake locations preferentially close to HF wells. Sensitivity of the results to a greater degree of spatial randomization (i.e., 50 km) is tested in Appendix B, in which we show that a larger distance perturbation for spatial randomization results in fewer hits in the simulated catalogs, thereby slightly increasing the inferred association rates in the observed catalog (i.e., after correction for false positives).

We determine the number of HF wells that are associated with events (i.e., number of hits) for each simulated catalog using the weighting function for different values of W. Figure 7 displays the distribution of the number of HF wells that are hits in the simulated catalogs for various values of W, in comparison with the corresponding number in the real catalog. In both the real and simulated catalogs, we count each well that registers as a hit only once to avoid double counting of wells. In Figure 7, we observe that all values of $W \geq 0.15$ (the minimum value we consider as potentially significant) result in an average number of hits in the simulated catalogs that is lower than the corresponding number in the real catalog. However, we note that for $W = 0.15$ the significance of the discrepancy is marginal. The value of $W = 0.15$ results in a hit rate that is not much greater than what we would expect by random chance. For $W \geq 0.25$, the number of hits in the real catalog exceeds the 99th percentile of hit rates in the simulated catalogs.

Because we increase the value of W that is used as the hit criterion, we decrease the number of hits in both the real and simulated catalogs, while increasing the separation between the distribution of false positives and the observed hit rate. We consider the true association rate to be measured by the difference between the observed hit rate and that expected by random chance; this is the observed hit rate minus the average hit rate for the randomized simulated catalogs. For example, based on the statistics shown in Figure 7, for $W = 0.25$, 0.35, and 0.50, we count 394, 308, and 225 hits in the real catalog respectively, which after subtracting the expected number of coincidental hits (240, 144, and 84, respectively) gives us a corrected count of 154, 164, and 141, respectively. This represents a stable association rate of ~0.7%$(= 100 \times 150/20,687)$. If we impose a higher confidence limit for association, considering the 99th percentile of the number of hits expected by random chance, the association rate would drop to about 0.5%.

In Figure 8, we show how the number of hits and the inferred association rates, after correcting for false positives, varies with the discriminant score. For low values of W (<0.2), the number of hits is high, but there is no clear distinction between the number observed in the real catalog and the

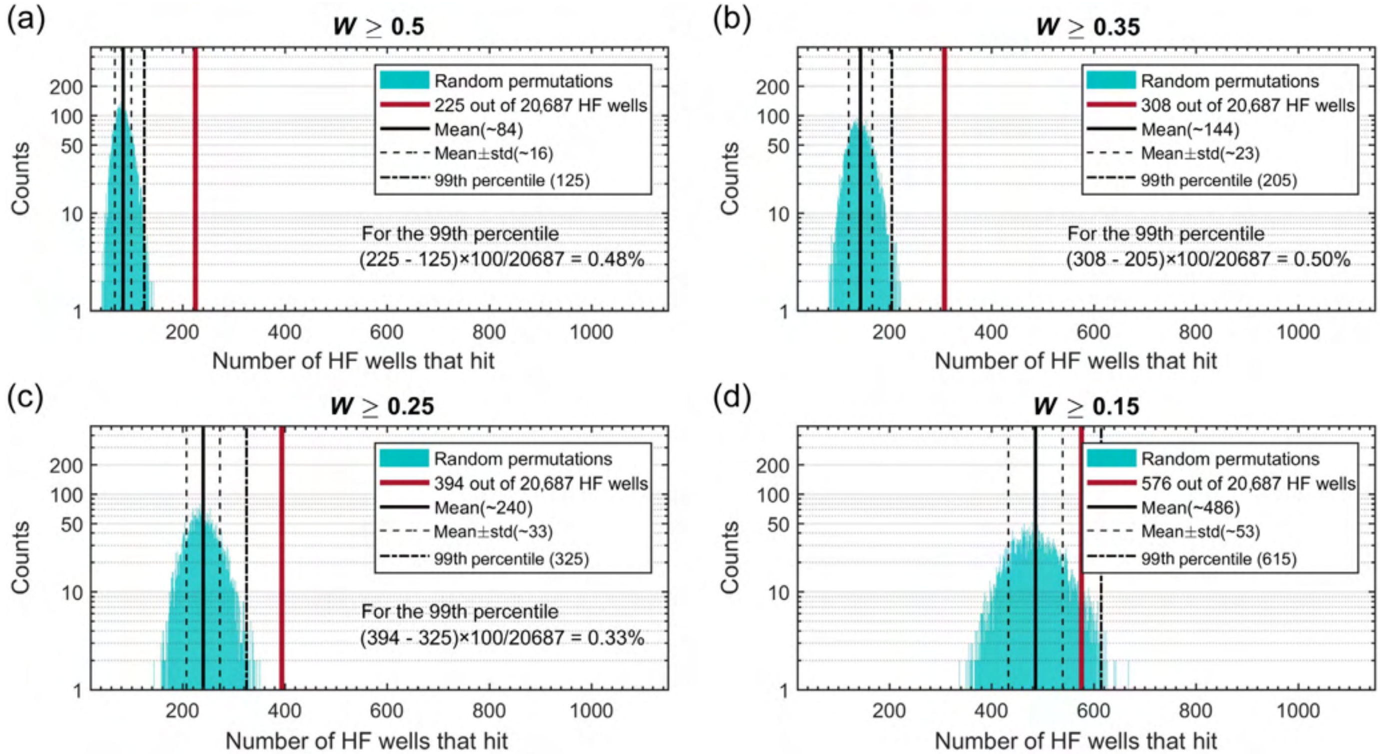

Figure 7. Histograms of number of hits for 5000 random realizations of the catalog (in which the locations and dates have been randomized as described in the Significance of the Observed Association of **M** ≥ 3 with HF Wells section), for (a–d) four values of the discriminant score W. The black solid and dashed lines are the mean and ±1 standard deviation of the number of hits in the simulated catalogs, with the 99th percentiles shown as dashed–dotted lines. The red vertical line is the corresponding hit rate for the real catalog (which increases with decreasing W). The radius of perturbation is from 0 to 20 km. The color version of this figure is available only in the electronic edition.

average number expected by chance (simulated catalogs). A stable separation between the hit rates in the real catalog and the values expected by chance emerges as W is increased, allowing for calculation of the association rate (shown as a percentage in Fig. 8). Our best estimate of the average regional association rate for $\mathbf{M} \geq 3$ earthquakes and HF wells, based on Figure 8, is ~0.7%–0.8%. This reflects the association rate after subtracting the average number of expected false positives for the range of W scores over which the separation between the numbers of hits in the real and simulated catalogs remains stable ($W \sim 0.25\text{–} \sim 0.50$). If we impose a higher level of confidence by subtracting the 99th percentile of false positives, we obtain an association rate of ~0.5%.

We summarize our conclusions regarding the association of HF wells with $\mathbf{M} \geq 3$ seismicity in the WCSB from 2009 to 2019 in Table 1, considering values of W of 0.5 and 0.35. We conclude, in consideration of our Monte Carlo results, that ~0.5%–1% of HF wells in the WCSB are associated with $\mathbf{M} \geq 3$ earthquakes and that about half of the observed seismicity in the region since 2009 can be attributed to HF wells.

In Table 1, we calculated the association rate using the number of hits under two alternative thresholds for the W score and subtracting the corresponding expected number of false positives. Another way we could think of this problem is that the W score implicitly contains a measure of the false positive rate, with $W = 0.5$ representing ~50% likelihood of association. As an alternative estimate of the regional association rate, we take the total number of HF wells that hit under a specified hit criterion (without double counting any HF well) n and divide it by the total number of candidate HF wells (N_T) to give us an initial estimate of the apparent association rate. We then consider that, to compensate for false positives, each hit should receive only partial weight, based on the strength of its association as measured by its W score. Thus, we multiply the initial apparent association rate by a partial weight factor W_p, which is defined for a specified discriminant value as the sum of the scores for all HF wells meeting the criterion ($\sum_{i=1}^{n_w} W$) divided by the corresponding number of associated HF wells (n_w):

$$W_p = \frac{\sum_{i=1}^{n_w} W}{n_w},$$

$$\text{Association}(\%) = 100 \times W_p \times \frac{n}{N_T}.$$

In summing partial weights, we include double-counted wells in the determination of W_p; thus $n_w > n$. For $W \geq 0.15$, the sum of the W scores from $n_w = 1110$ HF wells that meet the hit criterion is 438. The actual number of wells (i.e., no double counting) that are contributing to this total sum is $n = 576$.

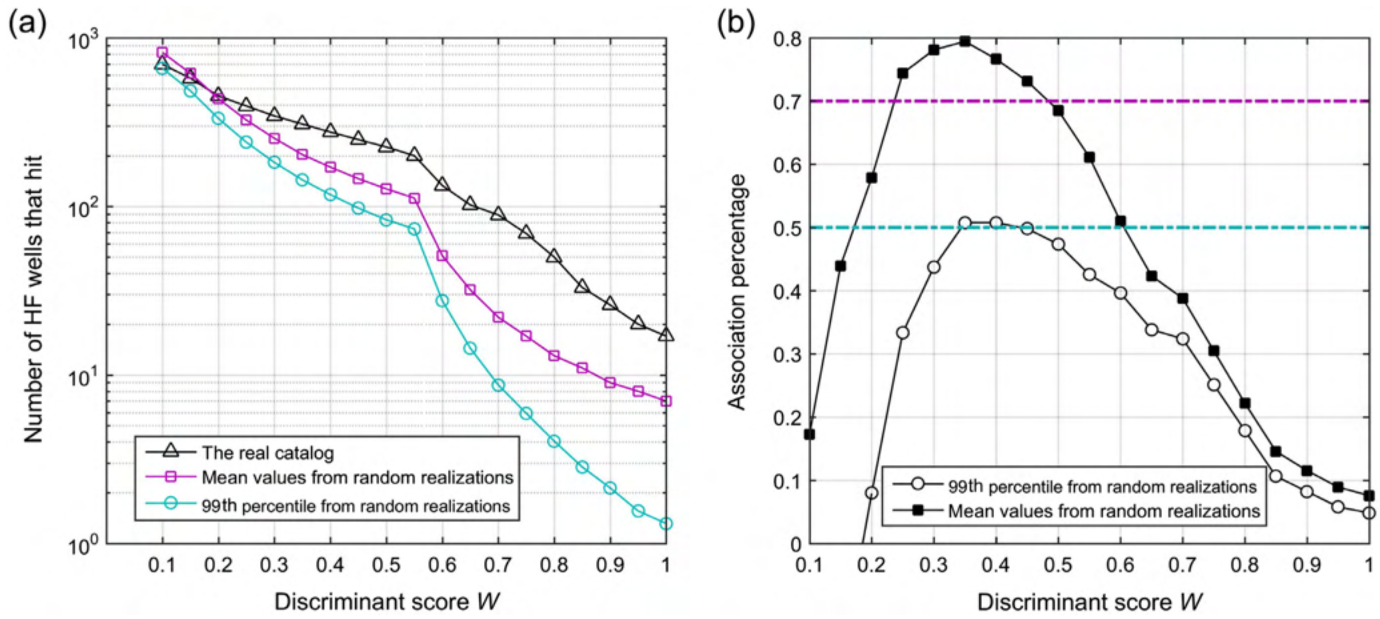

Figure 8. (a) Number of hits as a function of discriminant score W and (b) association percentage as a function of total discriminant score, for which association percentage is based on subtracting the expected number of false positives (from Fig. 7) from the hits, and then expressing as a percentage of total active wells. The score of 0.35 gives the highest discriminating power. The color version of this figure is available only in the electronic edition.

This gives an association rate of $1.10\%(= 100\times(438/1110)\times(576/20,687))$. If we include only those wells with $W \geq 0.25$, 0.35, or 0.50, then the sum of W scores will be 359, 314, or 245, respectively, from $n_w = 686$, 528, or 368, respectively. For the corresponding values (without double counting) of $n = 394$, 308, or 225, respectively, we obtain association rates of 1.0%, 0.9%, or 0.7%, respectively. The association rate is thus relatively stable with respect to the W-value, with a range from 1.1% to 0.7% for values of W in the range from 0.15 to 0.5; this is a reasonable range given the inherent uncertainty in calculating the association rate accurately.

The alternative approach to calculating the association rate, based on using the sum of weights as a tool to account for false positives, provides a simple association metric that replicates the results obtained using the more detailed Monte Carlo approach. This is useful for examining association metrics by formation, for which the statistics become sparse. We conclude that a stable and consistent regional association rate of ~0.8% per HF well (for $\mathbf{M} \geq 3$) is obtained under various reasonable alternative modeling choices. A simple approach that optimizes the use of sparse data is to calculate the association rate from the metric based on the average of the W values for all HF wells having $W \geq 0.15$.

DISCUSSION

The WCSB association rate of ~0.8% (from either the Monte Carlo or alternative calculation) is significantly higher than the value of 0.3% obtained by Atkinson *et al.* (2016) for the same region; this could reflect improved information to identify the association or growth in the association rate over time. Figure 9 explores the variability of the association rate in time using the simple association estimate based on summing W values,

TABLE 1
Summary of Seismicity Associated with HF Wells in the WCSB for $W \geq 0.5$ and $W \geq 0.35$

Parameters	Values	
Number of candidate wells (2009–2019)	20,687	
Discriminant score	0.5	0.35
Number of wells associated with $\mathbf{M} \geq 3$	225	308
Association percentage, accounting for false positive; 84 and 144 are the mean values for each score level from the Monte Carlo results	~0.7%$(= 225 - 84) \times 100/20,687$ (or 0.5% at 99th percentile confidence)	~0.8%$(= 308 - 144) \times 100/20,687$ (or 0.5% at 99th percentile confidence)
Number of $\mathbf{M} \geq 3$ (2009–2019)	152	
Percentage of $\mathbf{M} \geq 3$ (2009–2019) for HF wells	51%	55%

HF, hydraulic fracturing; WCSB, Western Canada Sedimentary Basin.

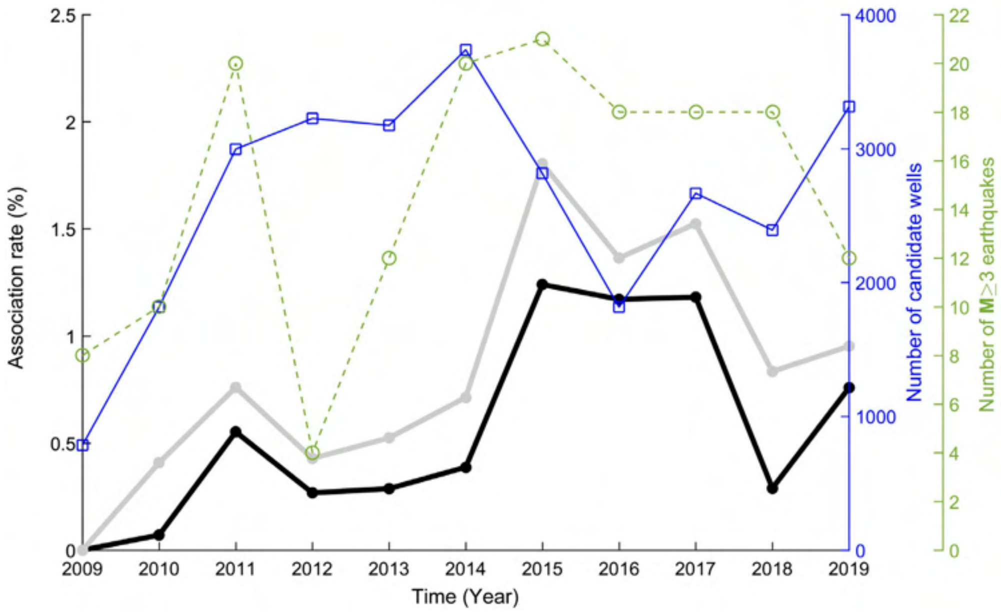

Figure 9. Variability of the estimated association rate in time. Left axis provides association rate in percentage ($W \geq 0.5$ shown as thick black lines and $W \geq 0.15$ shown as thick gray lines). Right axis provides number of candidate wells for the same time periods, along with number of $\mathbf{M} \geq 3$ earthquakes. Note that values for 2019 have been scaled by a factor of 4 because only the first 3 months of the year were considered (except for association percentage, which is invariant to scaling). The color version of this figure is available only in the electronic edition.

considering $W \geq 0.15$ and $W \geq 0.5$. We observe a rapid increase in the association rate from 2009 to 2011, during which time the number of HF wells and earthquakes per year also ramped up. From 2011 onward, temporal trends are unclear and the year-to-year variability is significant. The association rate appears to have slowly risen since 2010, although this observation may be biased by a higher-than-average association rate in 2015–2017. This trend may explain why our regional average is higher than that obtained by Atkinson *et al.* (2016); their study did not include data beyond June 2015. Moreover, it is believed that the HF well database in this study is more complete than that available to Atkinson *et al.* (2016) due to improvements in HF treatment databases. Finally, we note that there is no obvious correlation between the obtained association rates and the numbers of wells; the high-association rates for 2015–2017 correspond to an average number of HF wells. This lack of correlation between number of HF wells and association rate is further evidence that the association rates are robust and not significantly influenced by false positives.

We observe that the incidence of HF-triggered seismicity varies widely across the WCSB (Fig. 10), which is consistent with the results of previous studies (e.g., Atkinson *et al.*, 2016; Ghofrani and Atkinson, 2016; Schultz *et al.*, 2016). The reasons that susceptibility varies are not yet completely understood. There is a consensus view that a minimum requirement for a significant induced event is the nearby presence of a pre-existing critically stressed fault (Eaton, 2018). However, the details of how close the fault needs be, whether it needs to be optimally oriented for failure, and how or if such faults can be identified prior to activation are all under debate. Moreover, the conditions for triggering fault reactivation and the time and distance scales over which they operate may vary significantly with the mechanism by which seismicity is being caused. Specifically, causative mechanisms known to date include pore-pressure diffusion, Coulomb stress transfer, and stress transfer via aseismic creep (Eaton, 2018). The impact of elevated pore pressure should be constrained close to the well by low-formation permeabilities and would have a time scale governed by pore-pressure diffusion. However, other mechanisms may allow the stress effects of HF to be transferred to greater distances, on time scales that outpace that of pore-pressure diffusion. Observations suggest that seismicity has been triggered hundreds of meters above (e.g., Eyre *et al.*, 2019) or below (e.g., Friberg *et al.*, 2014; Schultz, Mei, *et al.*, 2015; Skoumal *et al.*, 2015; Bao and Eaton, 2016) the target formation and at distances of ~1–2 km laterally from the well (e.g., Schultz, Stern, *et al.*, 2015; Bao and Eaton, 2016; Igonin *et al.*, 2019).

Several previous studies have searched for geologic proxies that indicate regions of higher susceptibility. Within the WCSB, Schultz *et al.* (2016) noted that confirmed cases of induced earthquakes in central Alberta were preferentially focused in a narrowband along the margins of the Paleozoic reef complexes, known as the Swan Hills Formation. They conjectured that the association is likely due to (1) reef nucleation being a proxy marker for the presence of basement faults and/or (2) enhanced permeability and porosity from diagenesis. Eaton and Schultz (2018) documented two examples of strongly clustered HF seismicity within areas characterized by a steep pore-pressure gradient in the Montney and Duvernay Formations; they concluded that overpressured formations are more susceptible to induced seismicity, presumably because the elevated pore pressure reduces effective normal stress on faults. Pawley *et al.* (2018) found that a selection of features including proximity to basement, in situ stress, proximity to fossil reef margins, lithium concentration, and rate of natural seismicity, were among the strongest predictor

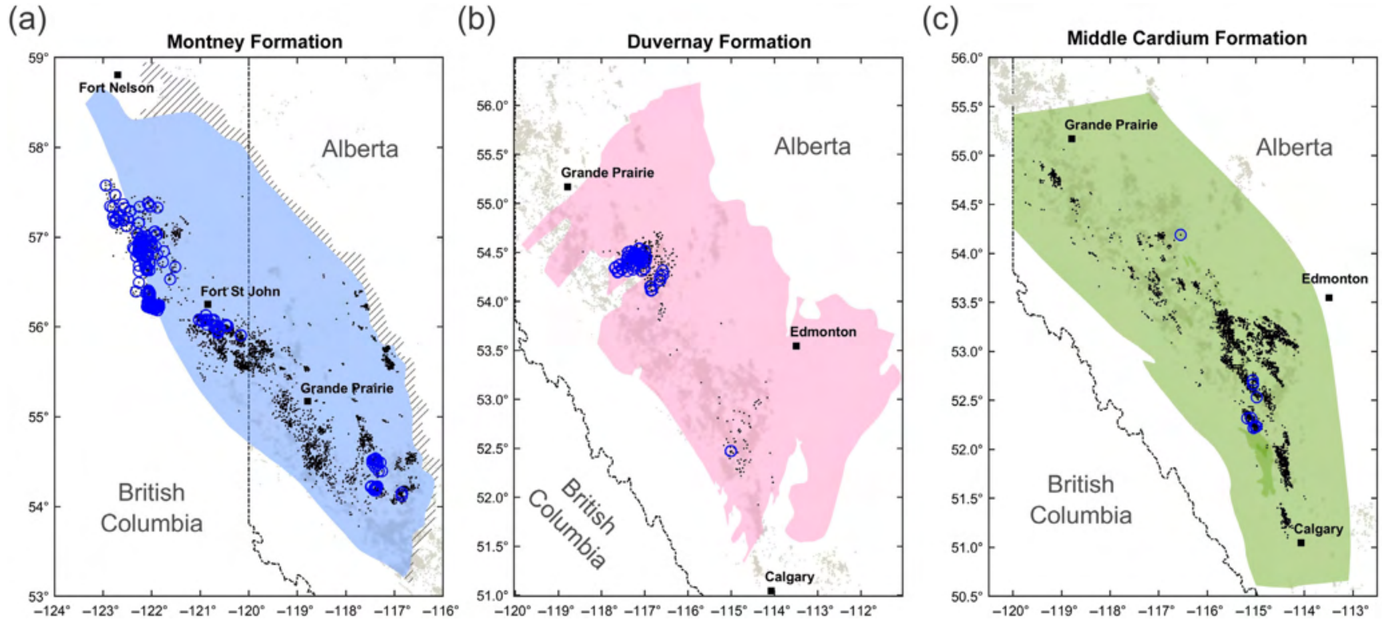

Figure 10. Distribution of all HF wells (gray dots) and the ones within (black dots) (a) Montney, (b) Duvernay, and (c) Cardium formations. Larger open circles show HF wells within each of these formations with $W \geq 0.15$. The color version of this figure is available only in the electronic edition.

variables for geological susceptibility to induced earthquakes in the Duvernay play.

Operational factors may also play an important role in earthquake susceptibility and productivity. Large injection volumes may affect a larger area and thus enhance the likelihood that stress perturbations reach critically stressed faults. Moreover, it has been shown that near Fox Creek, Alberta, earthquake productivity scales with injected volume (Schultz *et al.*, 2018). However, it is noteworthy that to date predictive tools based on geologic indicators or operational factors have not had much success in predicting future events. For example, the induced events of **M** 3–4 in 2018–2019 near Red Deer, Alberta (Schultz *et al.*, 2019), occurred in an area that had not previously been identified as susceptible based on geologic indicators.

Cases of well-documented HF seismicity within the WCSB have been most prevalent in the Duvernay and Montney Formations (e.g., Eaton, 2018). However, HF seismicity has been observed in many tectonic settings around the world, including in Ohio (Friberg *et al.*, 2014; Skoumal *et al.*, 2015), Oklahoma (Holland, 2013; Skoumal *et al.*, 2018), England (Clarke *et al.*, 2014), Poland (López-Comino *et al.*, 2017, 2018), and China (Lei *et al.*, 2019). To our knowledge, no geologic formation is immune to induced seismicity, but some formations have had a high incidence of induced events, whereas other formations appear to have seen negligible induced seismicity to date. In the following section, we subdivide our results by geological formation.

Subdivision of association rates by geological formation

The HF wells in the study area correspond to hydraulic fracture treatments in about 100 geological formations, ranging in age from Cretaceous to Devonian (∼70–400 million yr). The formation at the injection level (which is also the production level) is available in our database for 20,103 wells. There are 12 formations having at least one well with $W \geq 0.15$. These formations, along with their association rates as calculated from the simple metric based on partial weights (described previously), are listed in Table 2. Figure 10 shows the geographic locations of HF wells and hits for several major formations (Montney, Duvernay, Cardium, and Horn River Basin). In Figure 11, we show details of all hits in time–distance space for selected formations, whereas in Figure 12 we plot histograms of the number of wells and hits, ordered from younger to older formations. More than half of the HF wells were drilled in either the Montney (∼35%) or Cardium (∼22%) Formations. Although the largest number of hits is for the Montney, the highest association rate in percentage is for the Duvernay (∼6%), with the Montney having an association rate of ∼2%. The association rate for the Cardium is much lower at ∼0.07%. The relative susceptibility is observed to vary by formation in the WCSB by more than an order of magnitude. In a similar vein, Dinske and Shapiro (2013) characterized the rate of induced seismicity by calculating the seismogenic index (Shapiro *et al.*, 2010) across a selection of unconventional gas and geothermal reservoirs; they documented variability in susceptibility by over 10 orders of magnitude between different sites.

We note that for many formations there are no observed hits even for the 0.15 discriminant. We have not listed these formations to avoid any misinterpretation. Specifically, if no correlation has yet been observed, we deduce that the rate is

TABLE 2
Summary of the Number of All Wells and the Association Percentage for Formations Having Wells with $W \geq 0.5$, 0.35, 0.25, and 0.15

Formations	Composition (Lithology) (Age Range)‡	Total Number of Wells	Number of HF Wells [Sum of Scores] for $W \geq$ 0.5	0.35	0.25	0.15	Highest Score	Association Percentage for $W \geq$ 0.5	0.35	0.25	0.15
Duvernay	Shale/limestone, Frasnian (383–372 Ma)	751	61 [109.8]	67 [124.2]	70 [133.0]	112 [158.9]	1.0	5.5	5.7	5.5	6.4
Montney	Siltstone/shale/sandstone, Lower Triassic (252–247 Ma)	7142	129 [90.6]	188 [122.4]	252 [147.6]	362 [183.7]	1.0	1.2	1.5	1.7	1.9
Cardium	Sandstone/shale, Late Cretaceous (101–66 Ma)	4549	2 [1.1]	4 [2.3]	5 [3.0]	11 [4.2]	0.55	0.02	0.04	0.05	0.07
Muskwa*	Shale, Frasnian (383–372 Ma)	126	9 [15.0]	15 [22.3]	20 [26.6]	23 [31.6]	1.0	4.6	6.5	7.6	7.2
Evie member*	Shale, Middle Devonian (393–388 Ma)	61	10 [12.6]	10 [17.7]	10 [20.4]	12 [21.9]	1.0	10.8	9.3	8.4	9.2
Otter Park member*	Shale, Upper Devonian (383–372 Ma)	48	4 [5.5]	6 [8.4]	9 [9.3]	10 [12.6]	0.96	5.7	7.0	9.7	7.7
Dunvegan	Sandstone/shale, Cenomanian (101–94 Ma)	480	5 [5.7]	6 [6.9]	9 [7.7]	14 [8.7]	0.68	0.7	0.7	1.0	1.3
Gething	Sandstone/shale or mudstone/coal, Lower Cretaceous (125–113 Ma)	65	0 [0.0]	1 [0.5]	2 [0.7]	3 [1.9]	0.48	0.0	0.7	1.1	1.3
Cadomin Formation	Conglomerate/sandstone/shale/coal, Early Cretaceous (129–125 Ma)	122	0 [0.0]	0 [0.0]	1 [0.3]	1 [0.7]	0.31	0.0	0.0	0.3	0.2
Glauconitic sandstone†	Sandstone/shale Cretaceous (145–66 Ma)	865	0 [0.0]	0 [0.0]	1 [0.3]	2 [0.7]	0.29	0.0	0.0	0.03	0.05
Doig phosphate beds	Siltstone/shale, Middle Triassic (247–237 Ma)	373	0 [0.0]	0 [0.0]	0 [0.0]	3 [0.6]	0.20	0.0	0.0	0.0	0.2
Basal Belly River sandstone	Sandstone/bentonite/coal/shale, Late Cretaceous (101–66 Ma)	111	0 [0.0]	0 [0.0]	1 [0.3]	1 [0.3]	0.30	0.0	0.0	0.3	0.3

*Horn River Basin.
†Mannville group.
‡General description and approximate age of formation in millions of years before present (Million years; Ma) summarized from Alberta Table of Formations (see Data and Resources).

likely to be lower than that for the listed formations, but we do not know that it is zero. For example, if we had used a lower magnitude level ($\mathbf{M} \geq 2$), then we would have obtained hits in other formations and might potentially have obtained a more complete picture of susceptible formations. The use of a lower magnitude threshold would also increase our sample size for analysis and improve the statistical significance of results. This would be feasible if enhanced catalogs were compiled based on template matching or other analysis techniques that improve the magnitude of completeness. Improvement in the completeness and timeliness of the well database would also be helpful. Although susceptibility is widely variable, we have no reason to believe that any formations are immune to the potential for induced seismicity. Rather, we can only report and interpret the observations to date.

CONCLUSIONS

We examined the association between HF and $\mathbf{M} \geq 3$ earthquakes in the WCSB from 2009 to 2019. This is a significant update on an earlier study by Atkinson *et al.* (2016) that takes advantage of new information of HF wells and seismicity to develop a more robust discrimination algorithm. Our main conclusions are as follows:

1. As a basin-wide average, approximately 0.5%–1.0% of HF wells in the WCSB are associated with $\mathbf{M} \geq 3$ earthquakes. The association rate appears to have risen slowly over time.
2. There are eight geological formations (of >100) that have a documented association with $\mathbf{M} \geq 3$ earthquakes to date. Association rates for these formations are highly variable, being >5% for the Duvernay and <0.1% for the Cardium. The association rates are not correlated with the number of HF wells within each formation.
3. We have no reason to believe that any formation is immune to the potential for induced seismicity. However, there are many formations with no associated $\mathbf{M} \geq 3$ earthquakes to date.

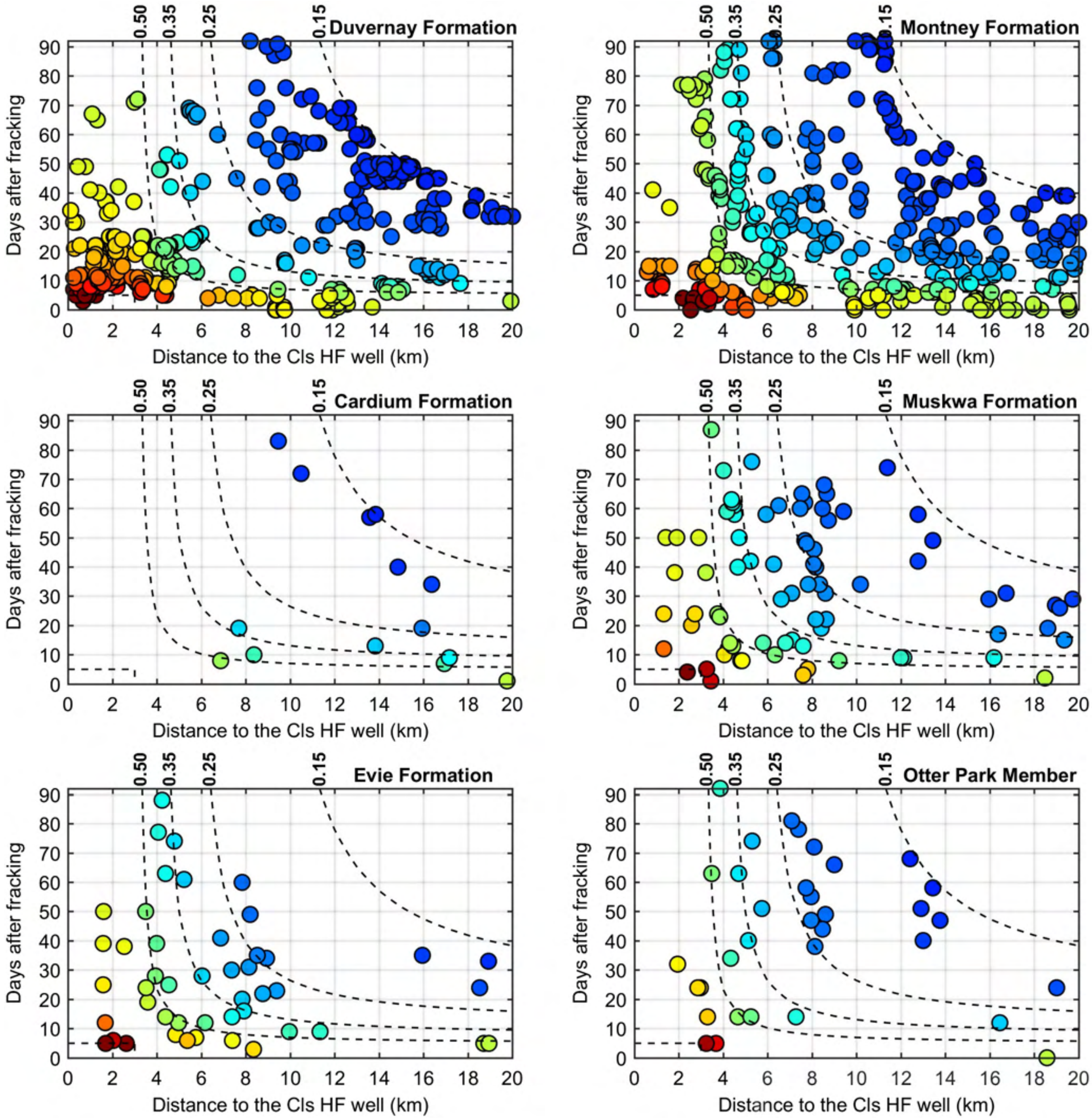

Figure 11. HF wells associated with $\mathbf{M} \geq 3$ seismicity for selected formations reported in Table 2. Shading is darker for higher values of W, as in Figure 6. The color version of this figure is available only in the electronic edition.

DATA AND RESOURCES

The database of ~700,000 wells (all types) was searched using geoSCOUT software (geoLOGIC systems Ltd.) licensed to Western University. The earthquake database was compiled from the Composite Seismicity Catalogue for Alberta and British Columbia for the 1 January 2009–30 April 2019 time period, available at www.inducedseismicity.ca (last accessed March 2020). All plots are produced with MATLAB available at www.mathworks.com/products/matlab (last accessed April 2020). The boundaries of the formations are obtained from Geological Atlas of the Western Canada Sedimentary Basin (WCSB) available at http://ags.aer.ca/reports/atlas-of-the-western-canada-sedimentary-basin.htm (last accessed April 2020). Information on geological formations was summarized from Alberta Geological Survey at https://ags.aer.ca/activities/table–of-formation.htm (last accessed April 2020). The Canadian Induced Seismicity Collaboration research program is focused on understanding the mechanisms and hazards associated with industry-related induced seismicity (www.inducedseismicity.ca, last

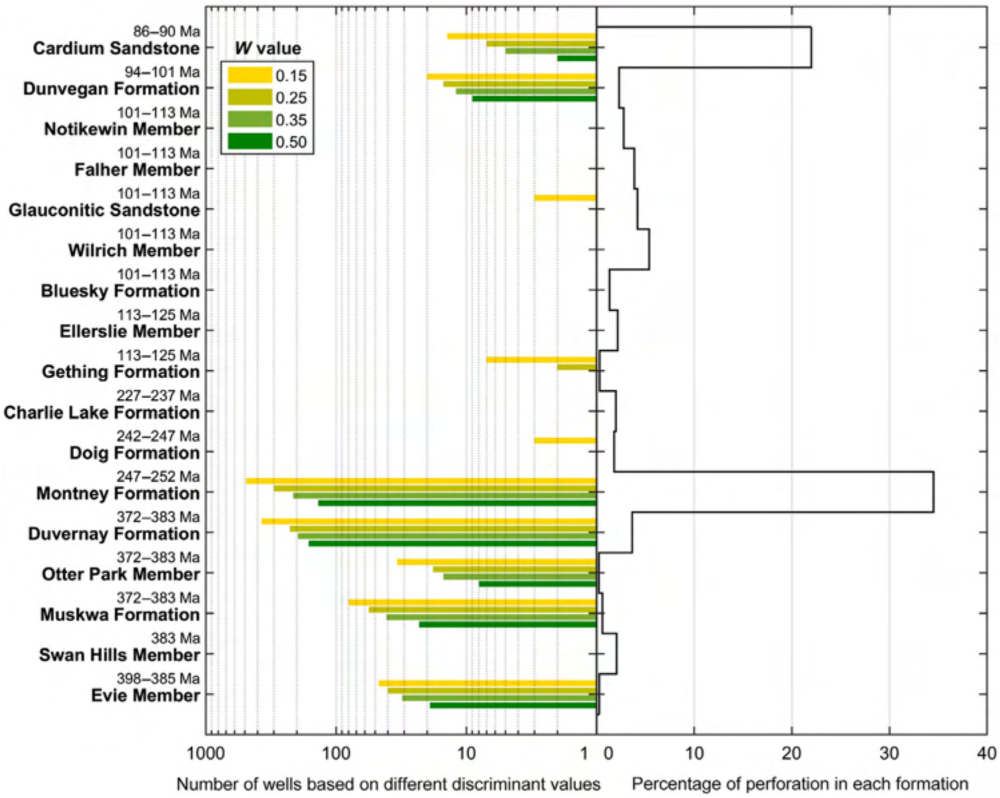

Figure 12. Number of wells based on different threshold values for W discriminant (shown in the legend) and percentage of wells in each formation. The formations are shown in ascending order based on age. We count all HF wells that pass the considered minimum score of W (so some wells may be double-counted). The color version of this figure is available only in the electronic edition.

accessed April 2020). B.C. Oil and Gas Commission (2012), "Investigation of observed seismicity in the Horn River Basin," available at https://www.bcogc.ca/node/8046/download (last accessed April 2020). B.C. Oil and Gas Commission (2014), "Investigation of observed seismicity in the Montney trend," available at https://www.bcogc.ca/node/12291/download (last accessed April 2020). B.C. Oil and Gas Commission (2015), "August seismic event determination, industry bulletin 2015-32," available at https://www.bcogc.ca (last accessed April 2020).

ACKNOWLEDGMENTS

Funding from the Natural Sciences and Engineering Research Council and TransAlta is gratefully acknowledged. The authors thank Editor-in-Chief Thomas Pratt, Guest Editor Cornelius Langenbruch, and two reviewers, Thomas Eyre and Rob Skoumal, for their constructive comments that led to improvements in the article.

REFERENCES

Atkinson, G. M. (2017). Strategies to prevent damage to critical infrastructure due to induced seismicity, *FACETS* **2,** 374–394, doi: 10.1139/facets-2017-0013.

Atkinson, G. M., D. W. Eaton, H. Ghofrani, D. Walker, B. Cheadle, R. Schultz, R. Shcherbakov, K. Tiampo, J. Gu, R. M. Harrington, *et al.* (2016). Hydraulic fracturing and seismicity in the Western Canada Sedimentary Basin, *Seismol. Res. Lett.* **87,** no. 3, 631–664, doi: 10.1785/0220150263.

Atkinson, G. M., H. Ghofrani, and K. Assatourians (2015). Impact of induced seismicity on the evaluation of seismic hazard: Some preliminary considerations, *Seismol. Res. Lett.* **86,** no. 3, 1009–1021, doi: 10.1785/0220140204.

Babaie Mahani, A. B., H. Kao, G. M. Atkinson, K. Assatourians, K. Addo, and Y. Liu (2019). Ground-motion characteristics of the 30 November 2018 injection-induced earthquake sequence in northeast British Columbia, Canada, *Seismol. Res. Lett.* **90,** no. 4, 1457–1467, doi: 10.1785/0220190040.

Bao, X., and D. W. Eaton (2016). Fault activation by hydraulic fracturing in western Canada, *Science* **354,** 1406–1409, doi: 10.1126/science.aag2583.

Brown, M. R. M., and S. Ge (2018). Distinguishing fluid flow path from pore pressure diffusion for induced seismicity, *Bull. Seismol. Soc. Am.* **108,** no. 6, 3684–3686, doi: 10.1785/0120180149.

Catalli, F., M. A. Meier, and S. Wiemer (2013). The role of Coulomb stress changes for injection-induced seismicity: The Basel enhanced geothermal system, *Geophys. Res. Lett.* **40,** 72–77, doi: 10.1029/2012GL054147.

Clarke, H., L. Eisner, P. Styles, and P. Turner (2014). Felt seismicity associated with shale gas hydraulic fracturing: The first documented example in Europe, *Geophys. Res. Lett.* **41,** 8308–8314, doi: 10.1002/2014GL062047.

Corlett, H., R. Schultz, P. Branscombe, T. Hauck, K. Haug, K. MacCormack, and T. Shipman (2018). Subsurface faults inferred from reflection seismic, earthquakes, and sedimentological relationships: Implications for induced seismicity in Alberta, Canada, *Mar. Petrol. Geol.* **93,** 135–144, doi: 10.1016/j.marpetgeo.2018.03.008.

Cui, L., and G. M. Atkinson (2016). Spatiotemporal variations in the completeness magnitude of the Composite Alberta Seismicity Catalog (CASC), *Seismol. Res. Lett.* **87,** no. 4, 853–863, doi: 10.1785/0220150268.

Dinske, C., and S. Shapiro (2013). Seismotectonic state of reservoirs inferred from magnitude distributions of fluid-induced seismicity, *J. Seismol.* **17,** 13–25, doi: 10.1007/s10950-012-9292-9.

Eaton, D. (2018). *Passive Seismic Monitoring of Induced Seismicity: Fundamental Principles and Application to Energy Technologies*, Cambridge University Press, Cambridge, United Kingdom, doi: 10.1017/9781316535547.

Eaton, D. W., and R. Schultz (2018). Increased likelihood of induced seismicity in highly overpressured shale formations, *Geophys. J. Int.* **214,** no. 1, 751–757, doi: 10.1093/gji/ggy167.

Eaton, D. W., N. Igonin, A. Poulin, R. Weir, H. Zhang, S. Pellegrino, and G. Rodriguez (2018). Induced seismicity characterization during hydraulic fracture monitoring with a shallow-wellbore geophone array and broadband sensors, *Seismol. Res. Lett.* **89,** no. 5, 1641–1651, doi: 10.1785/0220180055.

Ellsworth, W. (2013). Injection-induced earthquakes, *Science* **341,** no. 5142, 1225942, doi: 10.1126/science.1225942.

Ellsworth, W. L., A. L. Llenos, A. F. McGarr, A. J. Michael, J. L. Rubinstein, C. S. Mueller, M. D. Petersen, and E. Calais (2015). Increasing seismicity in the U.S. midcontinent: Implications for earthquake hazard, *The Leading Edge* **34,** no. 6, 618–626, doi: 10.1190/tle34060618.1.

Eyre, T., D. Eaton, D. Garagash, M. Zecevic, M. Venieri, R. Weir, and D. Lawton (2019). The role of aseismic slip in hydraulic fracturing-induced seismicity, *Sci. Adv.* **5,** no. 8, eaav7171, doi: 10.1126/sciadv.aav7172.

Frankel, A. (1995). Mapping seismic hazard in the Central Eastern United States, *Seismol. Res. Lett.* **66,** no. 4, 8–21, doi: 10.1785/gssrl.66.4.8.

Friberg, P. A., G. M. Besana-Ostman, and I. Drivker (2014). Characterization of an earthquake sequence triggered by hydraulic fracturing in Harrison County, Ohio, *Seismol. Res. Lett.* **85,** no. 6, 1295–1307, doi: 10.1785/0220140127.

Ghofrani, H., and G. M. Atkinson (2016). A preliminary statistical model for hydraulic fracture-induced seismicity in the Western Canada Sedimentary Basin, *Geophys. Res. Lett.* **43,** 10,164–10,172, doi: 10.1002/2016GL070042.

Ghofrani, H., G. M. Atkinson, R. Schultz, and K. Assatourians (2019). Short-term hindcasts of seismic hazard in the Western Canada Sedimentary Basin caused by induced and natural earthquakes, *Seismol. Res. Lett.* **90,** no. 3, 1420–1435, doi: 10.1785/0220180285.

Guglielmi, Y., F. Cappa, J.-P. Avouac, P. Henry, and D. Elsworth (2015). Seismicity triggered by fluid injection-induced aseismic slip, *Science* **348,** 1224–1226, doi: 10.1126/science.aab0476.

Holland, A. A. (2013). Earthquakes triggered by hydraulic fracturing in south-central Oklahoma, *Bull. Seismol. Soc. Am.* **103,** no. 3, 1784–1792, doi: 10.1785/0120120109.

Igonin, N., J. P. Verdon, J.-M. Kendall, and D. W. Eaton (2019). The role of parallel fracture networks for induced seismicity in the Duvernay Formation, *EAGE Annual Meeting*, London, United Kingdom, 3–7 June 2019, Expanded Abstracts WS16_07.

Kothari, S. (2019). Statistical modeling and characterization of induced seismicity within the Western Canada Sedimentary Basin, *Electronic Thesis and Dissertation Repository*, 6638 pp., available at https://ir.lib.uwo.ca/etd/6638 (last accessed April 2020).

Langenbruch, C., and A. A. Shapiro (2010). Decay rate of fluid-induced seismicity after termination of reservoir stimulations, *Geophysics* **75,** MA53–MA62, doi: 10.1190/1.3506005.

Lei, X., Z. Wang, and J. Su (2019). The December 2018 ML 5.7 and January 2019 ML 5.3 earthquakes in South Sichuan basin induced by shale gas hydraulic fracturing, *Seismol. Res. Lett.* **90,** no. 3, 1099–1110, doi: 10.1785/0220190029.

Lomax, A., and A. Savvaidis (2019). Improving absolute earthquake location in west Texas using probabilistic, proxy ground-truth station corrections, *J. Geophys. Res.* **124,** doi: 10.1029/2019JB017727.

López-Comino, J. A., S. Cesca, S. Heimann, F. Grigoli, K. Milkereit, T. Dahm, and A. Zang (2017). Characterization of hydraulic fractures growth during the Aspo Hard Rock Laboratory experiments (Sweden), *J. Rock Mech. Rock Eng.* **50,** no. 11, 2985–3001, doi: 10.1007/s00603-017-1285-0.

López-Comino, J. A., S. Cesca, J. Jaros lawski, N. Montcoudiol, H. Heimann, T. Dahm, S. Lasocki, A. Gunning, P. Capuano, and W. Ellsworth (2018). Induced seismicity response of hydraulic fracturing: Results of a multidisciplinary monitoring at the Wysin site, Poland, *Sci. Rep.* **8,** no. 1, 8653, doi: 10.1038/s41598-018-26970-9.

Murray, K. E. (2013). State-scale perspective on water use and production associated with oil and gas operations, Oklahoma, US, *Environ. Sci. Tech.* **47,** no. 9, 4918–4925, doi: 10.1021/es4000593.

Nur, A., and J. R. Booker (1972). Aftershocks caused by pore fluid flow? *Science*, New Series **175,** no. 4024, 885–887, doi: 10.1126/science.175.4024.885.

Pawley, S., R. Schultz, T. Playter, H. Corlett, T. Shipman, S. Lyster, and T. Hauck (2018). The geological susceptibility of induced earthquakes in the Duvernay play, *Geophys. Res. Lett.* **45,** no. 4, 1786–1793, doi: 10.1002/2017GL076100.

Pennington, C., and X. Chen (2017). Coulomb stress interactions during the Mw 5.8 Pawnee sequence, *Seismol. Res. Lett.* **88,** no. 4, 1024–1031, doi: 10.1785/0220170011.

Rubinstein, J. L., and A. Babaie Mahani (2015). Myths and facts on wastewater injection, hydraulic fracturing, enhanced oil recovery, and induced seismicity, *Seismol. Res. Lett.* **86,** no. 4, 1060–1067, doi: 10.1785/0220150067.

Schultz, R., and R. Wang (2020). Newly emerging cases of hydraulic fracturing induced seismicity in the Duvernay East Shale Basin, *Tectonophysics* **779,** 228393, doi: 10.1016/j.tecto.2020.228393.

Schultz, R., G. M. Atkinson, D. W. Eaton, Y. J. Gu, and H. Kao (2018). Hydraulic fracturing volume is associated with induced earthquake productivity in the Duvernay play, *Science* **359,** no. 6373, 304–308, doi: 10.1126/science.aao0159.

Schultz, R., H. Corlett, K. Haug, K. Kocon, K. MacCormack, V. Stern, and T. Shipman (2016). Linking fossil reefs with earthquakes: Geologic insight to where induced seismicity occurs in Alberta, *Geophys. Res. Lett.* **43,** 2534–2542, doi: 10.1002/2015GL067514.

Schultz, R., S. Mei, D. Pană, V. Stern, Y. J. Gu, A. Kim, and D. Eaton (2015). The Cardston earthquake swarm and hydraulic fracturing of the Exshaw Formation (Alberta Bakken play), *Bull. Seismol. Soc. Am.* **105,** no. 6, 2871–2884, doi: 10.1785/0120150131.

Schultz, R., S. M. Pawley, and T. E. Hauck (2019). Preliminary overview of the 2018 and 2019 earthquakes near Red Deer, Alberta; Alberta Energy Regulator/Alberta Geological Survey, *AER/AGS Open File Rept. 2019-12*, 10 pp.

Schultz, R., V. Stern, M. Novakovic, G. M. Atkinson, and Y. Gu (2015). Hydraulic fracturing and the Crooked Lake sequences: Insights gleaned from regional seismic networks, *Geophys. Res. Lett.* **42,** doi: 10.1002/2015GL063455.

Schultz, R., R. Wang, Y. J. Gu, K. Haug, and G. Atkinson (2017). A seismological overview of the induced earthquakes in the Duvernay play near Fox Creek, Alberta, *J. Geophys. Res.* **122,** 492–505, doi: 10.1002/2016JB013570.

Shapiro, S. A., C. Dinske, C. Langenbruch, and F. Wenzel (2010). Seismogenic index and magnitude probability of earthquakes induced during reservoir fluid stimulations, *The Leading Edge* **29,** no. 3, 304–309, doi: 10.1190/1.3353727.

Skoumal, R. J., M. R. Brudzinski, and B. S. Currie (2015). Earthquakes induced by hydraulic fracturing in Poland Township, Ohio, *Bull. Seismol. Soc. Am.* **105,** no. 1, 189–197, doi: 10.1785/0120140168.

Skoumal, R. J., R. Ries, M. R. Brudzinski, A. J. Barbour, and B. S. Currie (2018). Earthquakes induced by hydraulic fracturing are pervasive in Oklahoma, *J. Geophys. Res.* **123,** no. 12, 10,918–10,935, doi: 10.1029/2018JB016790.

Utsu, T., Y. Ogata, and R. Matsu'ura (1995). The centenary of the Omori formula for a decay law of aftershock activity, *J. Phys. Earth* **43,** 1–33, doi: 10.4294/jpe1952.43.1.

Viesca, R. C. (2015). Elastic stress transfer as a diffusive process due to aseismic fault slip in response to fluid injection, *American Geophysical Union Fall Meeting Abstracts*, San Francisco, California, 14–18 December 2015, MR41E–02.

Walsh, F. R., and M. D. Zoback (2015). Oklahoma's recent earthquakes and saltwater disposal, *Sci. Adv.* **1,** no. 5, e1500195, doi: 10.1126/sciadv.1500195.

Walter, W. R., K. M. Mayeda, and H. J. Patton (1995). Phase and spectral ratio discrimination between NTS earthquakes and explosions. Part I: Empirical observations, *Bull. Seismol. Soc. Am.* **85,** no. 4, 1050–1067.

Weingarten, M., S. Ge, J. W. Godt, B. A. Bekins, and J. L. Rubinstein (2015). High-rate injection is associated with the increase in US mid-continent seismicity, *Science* **345,** no. 6195, 448–451, doi: 10.1126/science.aab1345.

Zaliapin, I., and Y. Ben-Zion (2013). Earthquake clusters in southern California II: Classification and relation to physical properties of the crust, *J. Geophys. Res.* **118,** doi: 10.1002/jgrb.50178.

APPENDIX A

Discriminant scores for all study events having at least one well with $W \geq 0.15$, with cross references to literature.

TABLE A1
List of All M ≥ 3 Events for Which There Is At Least One Well with a Discriminant Score of ≥0.15

Date and Time (yyyy/mm/dd hh:mm)	Latitude (N)	Longitude (W)	M	Maximum Score	Reference ID
2010/06/11 22:25	59.502	122.303	3.3	0.45	1
2010/09/29 12:27	56.633	122.213	4.0	0.71	
2010/10/03 08:06	59.562	122.274	3.4	0.26	1
2010/10/05 22:01	59.598	122.394	3.5	0.23	1,10
2010/10/05 13:30	59.534	122.273	3.0	0.36	1,10
2010/10/08 20:14	53.123	116.020	3.0	0.30	5
2010/10/09 10:00	59.538	122.421	3.0	0.24	1,10
2010/10/12 17:09	59.589	122.451	3.3	0.19	1,10
2010/10/12 21:01	59.550	122.382	3.3	0.24	1,10
2011/02/04 19:18	56.999	122.256	3.3	0.88	5
2011/02/11 00:41	56.295	121.985	3.0	0.31	
2011/03/04 03:09	59.499	122.338	3.2	0.62	1
2011/04/07 12:19	59.499	122.507	3.1	0.63	1
2011/04/30 13:27	59.463	122.593	3.0	0.66	1
2011/05/03 12:56	59.514	122.321	3.1	0.47	1
2011/05/10 14:16	59.513	122.368	3.4	1.00	1
2011/05/19 13:05	59.489	122.405	3.6	0.67	1,10
2011/05/19 13:13	59.473	122.475	3.2	0.75	1,10
2011/05/29 08:09	59.537	122.463	3.0	0.67	1
2011/07/07 22:46	59.489	122.399	3.0	0.56	1,10
2011/10/29 12:40	56.272	121.880	3.0	0.50	
2011/11/04 03:37	56.522	122.179	3.1	0.20	
2011/12/12 23:34	59.812	122.678	3.0	1.00	1
2011/12/13 13:17	59.844	122.656	3.0	0.68	1,10
2012/05/11 13:04	56.224	122.058	3.3	0.61	5
2012/07/06 14:44	54.230	116.457	3.0	0.28	
2012/10/11 23:09	56.240	121.928	3.1	0.89	5
2013/04/07 02:39	56.342	121.852	3.4	0.34	5
2013/05/28 04:36	56.145	120.868	4.2	0.67	2
2013/08/21 15:31	56.907	122.000	3.3	0.73	2
2013/12/01 15:09	54.450	117.400	3.0	0.67	4,10

(*continued*)

TABLE A1 (*Continued*)

Date and Time (yyyy/mm/dd hh:mm)	Latitude (N)	Longitude (W)	M	Maximum Score	Reference ID
2013/12/01 01:38	54.499	117.385	3.0	1.00	4
2013/12/01 10:06	54.449	117.288	3.0	0.69	4,10
2014/01/02 20:34	54.487	117.289	3.0	0.60	4
2014/01/25 03:59	54.508	117.214	3.1	0.65	4
2014/03/01 04:35	56.449	121.449	3.4	0.19	5
2014/03/02 22:24	57.295	122.481	3.1	1.00	2
2014/05/14 09:46	54.508	117.340	3.1	0.38	4
2014/05/15 11:58	54.412	117.213	3.0	0.39	4
2014/07/13 09:12	52.233	115.245	3.1	0.31	
2014/07/16 17:44	57.268	122.727	3.6	0.60	2
2014/07/30 21:23	57.542	122.894	3.8	0.80	2
2014/08/04 17:17	57.564	122.942	4.4	0.81	2,10
2014/08/09 15:28	52.208	115.218	4.0	0.24	2
2014/12/17 10:01	56.444	121.596	3.6	0.20	
2014/12/21 00:18	56.533	122.242	3.0	0.22	
2014/12/29 15:03	56.335	121.905	3.2	0.32	5
2015/01/07 04:50	54.433	117.301	3.1	0.66	5,6
2015/01/07 05:28	54.429	117.301	3.2	0.66	5,6,10
2015/01/14 16:06	54.369	117.353	3.6	1.00	7,6
2015/01/15 19:18	54.381	117.457	3.3	0.70	5,6,10
2015/01/23 06:49	54.427	117.305	3.8	0.67	7,6,10
2015/02/10 07:39	54.368	117.223	3.0	1.00	7,6
2015/03/01 11:30	56.966	122.090	3.0	0.51	5
2015/06/02 14:34	52.447	114.989	3.3	0.56	
2015/06/13 23:57	54.148	116.862	4.0	0.94	7,4
2015/08/17 20:15	57.013	122.154	4.6	0.81	3
2015/08/19 00:02	54.476	117.257	3.0	0.81	7
2015/08/22 04:46	54.452	117.227	3.1	0.75	10
2015/08/28 03:52	56.650	121.621	3.5	0.27	
2015/09/01 08:00	54.459	117.225	3.1	0.65	10
2015/09/02 07:42	57.014	122.122	3.4	0.62	10
2015/09/04 13:23	54.460	117.242	3.0	0.64	10
2015/11/03 12:41	57.233	122.471	3.5	0.98	
2015/11/21 17:57	57.038	122.225	3.3	0.88	
2016/01/12 18:27	54.411	117.287	4.1	0.84	7
2016/03/10 02:37	56.965	122.091	3.0	0.73	
2016/07/12 21:08	57.374	122.023	3.9	0.93	
2016/10/16 03:27	57.184	122.718	3.4	0.84	
2016/11/10 05:58	56.353	121.954	3.0	0.17	
2016/11/10 03:05	54.339	117.257	3.1	0.71	
2016/11/25 21:24	54.352	117.244	3.5	1.00	8,10
2016/11/25 05:31	54.357	117.239	3.4	1.00	8
2016/11/28 06:53	54.353	117.269	3.0	0.84	8,10
2016/11/29 10:15	54.341	117.262	3.6	0.81	8,10
2016/11/29 04:12	54.355	117.241	3.0	0.81	8,10
2016/12/03 05:13	56.268	122.089	3.3	0.73	
2016/12/05 14:27	54.342	117.236	3.3	0.71	10
2016/12/06 01:05	54.345	117.242	3.3	0.70	10
2016/12/07 10:11	54.334	117.248	3.3	0.69	10
2016/12/30 00:06	56.591	122.379	3.1	0.17	
2017/01/16 18:23	54.310	117.594	3.0	0.77	
2017/06/25 22:56	54.423	117.424	3.3	1.00	
2017/06/28 19:00	54.424	117.430	3.1	0.84	10
2017/06/30 23:50	54.416	117.416	3.0	0.79	10
2017/10/23 01:28	56.698	122.150	3.1	0.71	
2017/10/27 04:18	56.357	122.105	3.0	0.77	
2017/11/15 19:13	56.812	122.227	3.0	1.00	

(*continued*)

TABLE A1 (*Continued*)

Date and Time (yyyy/mm/dd hh:mm)	Latitude (N)	Longitude (W)	M	Maximum Score	Reference ID
2017/11/18 08:45	57.251	122.706	3.5	0.60	
2017/12/05 16:01	54.228	116.631	3.2	0.81	
2017/12/07 13:28	54.243	116.639	3.1	0.77	10
2017/12/16 11:29	54.236	116.636	3.4	0.67	10
2018/01/25 02:31	56.749	121.798	3.6	0.48	
2018/04/30 05:06	56.075	120.188	3.0	0.16	
2018/05/19 07:56	56.321	121.828	3.0	0.16	
2018/06/27 10:23	54.364	117.720	3.2	0.88	
2018/07/03 19:44	54.235	117.857	3.4	0.33	10
2018/07/05 08:03	54.320	117.627	3.1	0.73	
2018/07/05 15:12	54.308	117.713	3.0	0.58	10
2018/07/11 08:38	54.327	117.620	3.2	0.67	10
2018/07/14 06:21	54.317	117.609	3.0	0.65	10
2018/08/26 02:59	54.299	117.645	3.0	0.58	
2018/11/30 01:27	56.041	120.676	3.9	0.49	9
2018/11/30 02:06	56.026	120.556	3.1	0.32	9
2018/11/30 02:15	56.115	120.615	3.7	0.18	9
2019/02/20 16:22	56.811	122.180	3.3	0.71	
2019/02/27 16:41	56.819	122.109	3.2	1.00	
2019/03/10 10:00	52.573	115.259	3.8	0.55	

The following are references to cases of hydraulic fracturing (HF) seismicity that have been discussed in the literature. The list is sorted in chronological order; major findings are summarized. The numbers correspond to the reference ID's in table. 1, B.C. Oil and Gas Commission (unpublished manuscript, 2012, see Data and Resources): Anomalous seismicity (M_L 2.2–3.8) in the Horn River Basin between April 2009 and December 2011 was investigated. The investigation concluded that the events were caused by fluid injection during HF in proximity to pre-existing faults. All events occurred during or between HF stage operations; 2, B.C. Oil and Gas Commission (unpublished manuscript, 2014, see Data and Resources): The commission investigated events recorded between August 2013 and October 2014 in the Montney. They found that during this period 231 seismic events were attributed to oil and gas operations—38 induced by wastewater disposal and 193 by HF operations. The commission identified five areas within the Montney where seismic events were linked to HF operations (Caribou, Beg-Town, Altares, Septimus, and Doe-Dawson); 3, B.C. Oil and Gas Commission (unpublished manuscript, 2015, see Data and Resources): The commission determined that an **M** 4.6 seismic event on 17 August 2015 in northeast British Columbia was caused by fluid injection during HF. Hydraulic fracture operations were ongoing from 11 August to 2 September 2015. The epicenter of the event was located to within one kilometer of the operator's wellbore using detailed data from a dense array and the Canadian National Seismograph Network (CNSN); 4, Schultz, Stern, *et al.* (2015): HF-induced seismicity was studied for the Duvernay Formation in central Alberta, near Fox Creek, from December 2013 to the end of 2014. The spatiotemporal clustering of events was shown to be strongly related to the nearby HF operations. It was concluded that the sequences were triggered by pore pressure increases in response to HF stimulations along previously existing faults; 5, Atkinson *et al.* (2016): This study classified **M** > 3 events into five categories including HF, disposal, tectonic, or some combination. We identify only events that were classified as HF-induced; 6, Bao and Eaton (2016): This was a detailed analysis of seismicity from December 2013 to March 2015 near Fox Creek, Alberta, which clearly linked HF operations to several distinct clusters of seismicity. The results from this study show evidence of activating pre-existing faults due to both pore pressure and stress perturbation mechanisms; 7, Schultz *et al.* (2017): This study examined events from January 2015 to February 2016 in the Duvernay Formation in central Alberta, near Fox Creek. They concluded that earthquakes in this region cluster into distinct sequences in time, space, and focal mechanism and are strongly related to the nearby HF operations; 8, Eaton *et al.* (2018): This study used continuous passive seismic data from the Tony Creek Dual Microseismic Experiment (ToC2ME) acquired from October to December 2016. This experiment monitored a four-well HF program within the Kaybob–Duvernay region of Alberta, Canada. The dataset included >4000 HF-triggered events with well-determined magnitudes and hypocenters, with a maximum magnitude of **M** 3.2; 9, Babaie Mahani *et al.* (2019): This study analyzed ground-motion characteristics of three felt earthquakes that occurred in November 2018 in the Septimus region of northeast British Columbia in connection with nearby HF operations; 10, Kothari (2019): This study of **M** ≥ 3 events in the Western Canada Sedimentary Basin (WCSB) from 1975 to 2018 used clustering properties as defined by Zaliapin and Ben-Zion (2013) (tightly clustered, loosely clustered, and background). They document a rise in the rates of tightly clustered earthquakes corresponding with the increase in HF activity, whereas loosely clustered activity corresponded with other types of anthropogenic operations (conventional production, waste water disposal, and in some cases HF). We identify only those events classified by Kothari as "tightly clustered." It should be noted that tectonic aftershock sequences are also capable of generating tightly clustered activity; thus this classification is not definitive.

APPENDIX B

Sensitivity of Monte Carlo results to spatial randomization

We explored the sensitivity of our Monte Carlo results to a greater spatial randomization of the epicentral locations in the catalog. One might argue that keeping the events within 20 km of their original locations (and thus close to the wells) could bias the estimated number of random associations on the high side. We repeated the Monte Carlo simulation using a random perturbation from 0 to 50 km. The results are shown in Figure B1. Increasing the distance scale of spatial randomization results in lower association rates in the simulated catalogs and therefore increases the estimated activation rates after correction for false positives. We obtain association rates of ~0.6% using the 99th percentile of the false positives or

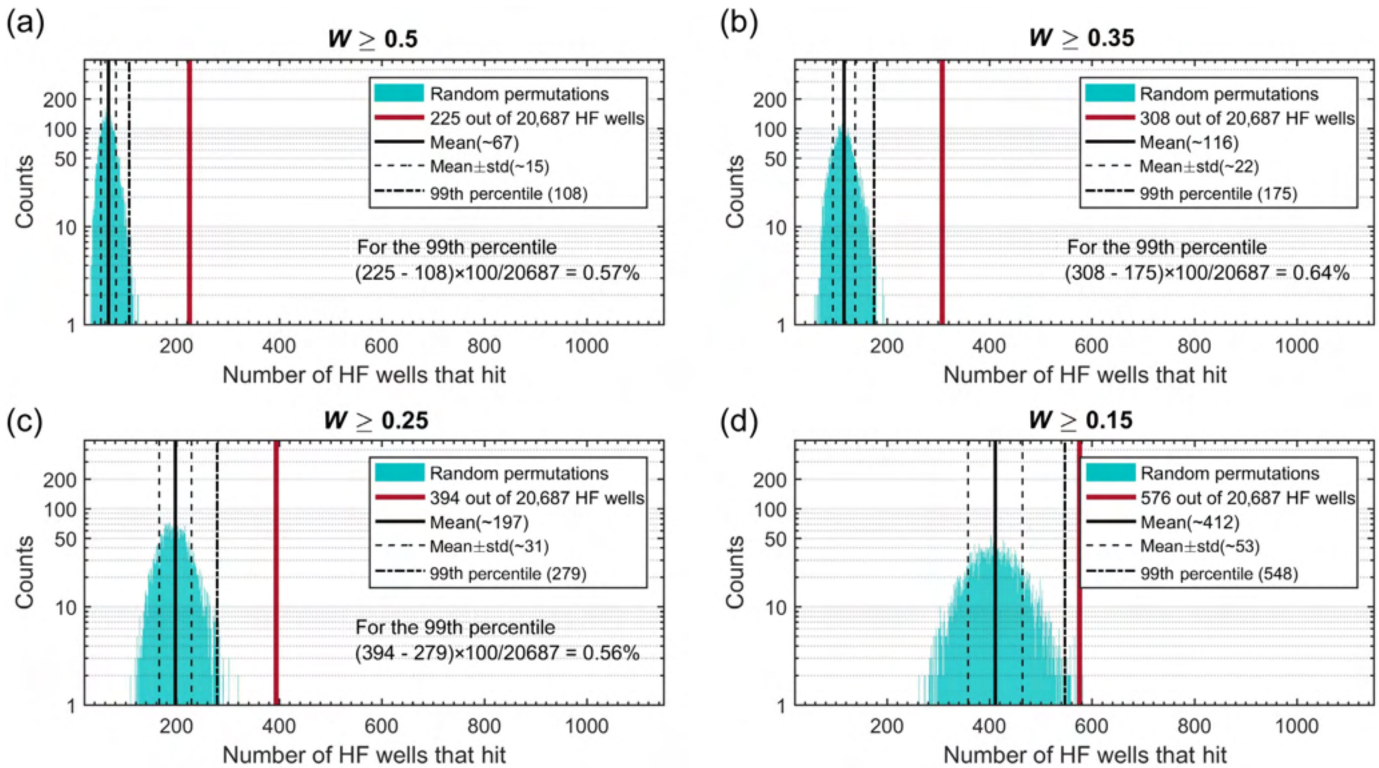

Figure B1. Histograms of number of hits for 5000 random realizations of the catalog (in which the locations and dates have been randomized as described in the Sensitivity of Monte Carlo Results to Spatial Randomization section), for (a–d) four values of the discriminant score W. The black solid and dashed lines are the mean and ± 1 standard deviation of the number of hits in the simulated catalogs, with the 99th percentiles shown as dashed–dotted lines. The red vertical line is the corresponding hit rate for the real catalog (which increases with decreasing W). The radius of perturbation is from 0 to 50 km. The color version of this figure is available only in the electronic edition.

~0.9% using the expected number of false positives. This supports our conclusion that the true regional association rate of hydraulic fracturing (HF) wells with $\mathbf{M} \geq 3$ earthquakes for the Western Canada Sedimentary Basin (WCSB) (from 2009 to 2019) lies within the range from 0.5% to 1.0%.

Manuscript received 5 January 2020
Published online 12 May 2020